Manuscript submitted to
AIMS' Journals
Volume **X**, Number **0X**, XX **200X**

Website: http://AIMsciences.org

pp. **X–XX**

WELL-BALANCED SCHEMES USING ELEMENTARY SOLUTIONS FOR LINEAR MODELS OF THE BOLTZMANN EQUATION IN ONE SPACE DIMENSION

Dedicated to the memory of Carlo Cercignani (1939–2010).

Laurent Gosse

Istituto per le Applicazioni del Calcolo (sezione di Bari)
via G. Amendola, 122/D, 70126 BARI, Italy

(Communicated by the associate editor name)

Abstract. In the kinetic theory of gases, a class of one-dimensional problems can be distinguished for which transverse momentum and heat transfer effects decouple. This feature is revealed by projecting the linearized Boltzmann model onto properly chosen directions (which were originally discovered by Cercignani in the sixties) in a Hilbert space. The shear flow effects follow a scalar integro-differential equation whereas the heat transfer is described by a 2×2 coupled system. This simplification allows to set up the well-balanced method, involving non-conservative products regularized by solutions of the stationary equations, in order to produce numerical schemes which do stabilize in large times and deliver accurate approximations at numerical steady-state. Boundary-value problems for the stationary equations are solved by the technique of "elementary solutions" at the continuous level and by means of the "analytical discrete ordinates" method at the numerical one. Practically, a comparison with a standard time-splitting method is displayed for a Couette flow by inspecting the shear stress which must be a constant at steady-state. Other test-cases are treated, like heat transfer between two unequally heated walls and also the propagation of a sound disturbance in a gas at rest. Other numerical experiments deal with the behavior of these kinetic models when the Knudsen number becomes small. In particular, a test-case involving a computational domain containing both rarefied and fluid regions characterized by mean free paths of different magnitudes is presented: stabilization onto a physically correct steady-state free from spurious oscillations is observed.

Contents

2000 *Mathematics Subject Classification.* Primary 65M06, 35L65; Secondary 82B40,82C40.
Key words and phrases. slow rarefied flow, well-balanced scheme, elementary solutions, analytical discrete-ordinates method, integral equation of the third kind.

1. Introduction.

1.1. A short review of the Boltzmann equation.

Kinetic theory describes the time evolution of a gas (or any other system constituted of a huge number of indistinguishable particles) by means of a function of distribution in the phase space; usually it is denoted by $f(t, \mathbf{x}, \mathbf{v}) \in [0, 1]$, with $\mathbf{x} \in \mathbb{R}^3$ (or in a bounded domain in $\mathbb{R}^3$) and the velocity variable $\mathbf{v} \in \mathbb{R}^3$. The equation ruling the evolution of this density function has been written in 1872 by Boltzmann [69]:

$$\partial_t f + \mathbf{v}.\nabla f = Q(f, f)(t, \mathbf{x}, \mathbf{v}), \tag{1}$$

where "." stands for the scalar product in $\mathbb{R}^3$ and, in standard notation,

$$Q(f, g)(t, \mathbf{x}, \mathbf{v}) = \int_{\mathbb{R}^3} d\mathbf{v}^* \int_{\mathbb{S}^2_+} d\mathbf{n} B(|\mathbf{v} - \mathbf{v}_*|, \mathbf{n})(f' g'_* - f g_*).$$

We used the shorthand notation: $f = f(t, \mathbf{x}, \mathbf{v})$, $f' = f(t, \mathbf{x}, \mathbf{v}')$, $f_* = f(t, \mathbf{x}, \mathbf{v}_*)$, $f'_* = f(t, \mathbf{x}, \mathbf{v}'_*)$. When a collision occurs between 2 particles of velocities $\mathbf{v}$ and $\mathbf{v}_*$ respectively, it is asked that momentum and kinetic energy must be conserved throughout the process. However, even with this requirement, the system which produces the post-collision velocities $\mathbf{v}'$ and $\mathbf{v}'_*$ is under-determined. Hence one introduces the kernel $0 \leq B$ and the parameter $\mathbf{n} \in \mathbb{S}^2_+$, the unit vector in the direction of the apse-line bisecting the angle between $\mathbf{v} - \mathbf{v}_*$ and $\mathbf{v} - \mathbf{v}'_*$,

$$\mathbf{n} \in \mathbb{S}^2_+ := \left\{ \mathbf{n} \in \mathbb{R}^3 : \ |\mathbf{n}| = 1, \ \mathbf{n}.(\mathbf{v}_* - \mathbf{v}) \geq 0 \right\},$$

in order to solve:

$$\mathbf{v}' = \frac{1}{2}(\mathbf{v}+\mathbf{v}_*) + \frac{1}{2}|\mathbf{v}-\mathbf{v}_*|\mathbf{n}, \qquad \mathbf{v}'_* = \frac{1}{2}(\mathbf{v}+\mathbf{v}_*) - \frac{1}{2}|\mathbf{v}-\mathbf{v}_*|\mathbf{n}.$$

Collision kernels vary according to the models; the most classical one reads,

$$B(\mathbf{w},\mathbf{n}) = b|\mathbf{w}|^\gamma \cos(\theta), \qquad \cos(\theta) = \left(\frac{\mathbf{v}-\mathbf{v}_*}{|\mathbf{v}-\mathbf{v}_*|}.\frac{\mathbf{v}'-\mathbf{v}'_*}{|\mathbf{v}'-\mathbf{v}'_*|}\right),$$

where one speaks about soft (resp. hard) potentials when $\gamma < 0$ (resp. $\gamma > 0$). The "hard spheres" potential is the case where b is a constant and $\gamma = 1$. A more general expression for a collision kernel is given by: $B(\mathbf{w},\mathbf{n}) = \Phi(|\mathbf{w}|)b(\theta)$.

As a consequence of Boltzmann's H-theorem expressing time-irreversibility, entropy is dissipated as time passes and the solution f decays toward an equilibrium state which is the Maxwellian distribution, usually denoted by $M(\mathbf{v})$[1]. More precisely, one can multiply both sides of the equation (1) by $\log f$, integrate in $\mathbf{v} \in \mathbb{R}^3$,

$$\partial_t \int_{\mathbb{R}^3} f \log f d\mathbf{v} + \nabla. \int_{\mathbb{R}^3} \mathbf{v} f \log f d\mathbf{v} = \int_{\mathbb{R}^3} Q(f,f) \log f d\mathbf{v},$$

and observe that the right-hand side has a sign:

$$\int_{\mathbb{R}^3} Q(f,f)\log f d\mathbf{v} \leq 0,$$

with equality if and only if f is a Maxwellian. When f is assumed to be very close to this equilibrium state, it makes sense to consider $f = M(\mathbf{v})(1 + h(t,\mathbf{x},\mathbf{v}))$ with h satisfying the linearized equation with the simplified right-hand side:

$$\int_{\mathbb{R}^3} d\mathbf{v}^* \int_{\mathbb{S}^2_+} d\mathbf{n}\Phi(|\mathbf{v}-\mathbf{v}_*|)b(\theta)M(\mathbf{v}_*)(h' + h'_* - h - h_*). \tag{2}$$

A collision invariant is a function $\phi(\mathbf{v})$ for which the following equality holds:

$$\int_{\mathbb{R}^3} \phi(\mathbf{v})Q(f,f)d\mathbf{v} = 0.$$

A tedious computation allows to rewrite the preceding integral (see [23] page 14):

$$\int_{\mathbb{R}^3} \phi(\mathbf{v})Q(f,f)d\mathbf{v} = \frac{1}{2}\int_{\mathbb{R}^3}\int_{\mathbb{R}^3}\int_{\mathbb{S}^2_+} f f_*(\phi' + \phi'_* - \phi - \phi_*)B(|\mathbf{v}-\mathbf{v}_*|,\mathbf{n})d\mathbf{v}d\mathbf{v}_*d\mathbf{n}.$$

This integral vanishes independently of f if:

$$\phi' + \phi'_* = \phi + \phi_* \Leftrightarrow \phi(\mathbf{v}) = a + \mathbf{b}.\mathbf{v} + c|\mathbf{v}|^2, \quad a, \mathbf{b}, c \in \mathbb{R}\times\mathbb{R}^3\times\mathbb{R}.$$

This expression of the elementary collisional invariants allows to explicit the uniform Maxwellian distribution by arguing that $\log f$ must be a collisional invariant:

$$\log f = a + \mathbf{b}.\mathbf{v} + c|\mathbf{v}|^2 \Leftrightarrow f = \exp(a + \mathbf{b}.\mathbf{v} + c|\mathbf{v}|^2).$$

In order to get an integrable function, one must ask for $c \in \mathbb{R}_-$; hence by letting $c = -\beta$, $\mathbf{b} = 2\beta\mathbf{u}$ for some constant $\mathbf{u}$ and $\alpha \geq 0$, the Maxwellian states rewrite:

$$\forall \mathbf{v} \in \mathbb{R}^3, \qquad M(\mathbf{v}) = \alpha \exp(-\beta|\mathbf{v}-\mathbf{u}|^2), \qquad \mathbf{u} \in \mathbb{R}^3. \tag{3}$$

[1] The notation $M(\mathbf{v})$ refers to an "uniform Maxwellian" which doesn't depend on the variables $t, \mathbf{x}$. On the other hand, a "local Maxwellian" would be denoted by $M(t,\mathbf{x},\mathbf{v})$.

1.2. **Simplified models and their fluid dynamic approximation.** The usual macroscopic variables can be deduced as the successive moments of f in the $\mathbf{v}$ variable (particles are supposed to be of unit mass for simplicity):

$$\varrho(t,\mathbf{x}) = \int_{\mathbb{R}^3} f(t,\mathbf{x},\mathbf{v})d\mathbf{v}, \qquad \varrho\mathbf{u}(t,\mathbf{x}) = \int_{\mathbb{R}^3} \mathbf{v}f(t,\mathbf{x},\mathbf{v})d\mathbf{v},$$

which are respectively the gas density and its momentum in $t,\mathbf{x} \in \mathbb{R}_+ \times \mathbb{R}^3$. The internal energy, satisfying $\frac{2}{3}\varepsilon = kT$ with T the temperature and k stands for Boltzmann's constant[2], can be also defined as follows:

$$\varrho\varepsilon(t,\mathbf{x}) = \frac{1}{2}\int_{\mathbb{R}^3} |\mathbf{v} - \mathbf{u}(t,\mathbf{x})|^2 f(t,\mathbf{x},\mathbf{v})d\mathbf{v},$$

where $\mathbf{u}(t,\mathbf{x}) = \varrho\mathbf{u}(t,\mathbf{x})/\varrho(t,\mathbf{x})$ is called the bulk velocity of the gas and is defined as long as $\varrho(t,\mathbf{x}) > 0$. The quantity $\mathbf{c} := \mathbf{v} - \mathbf{u}$ is the zero-average deviation of the microscopic velocities with respect to the macroscopic one, called random or peculiar velocity. We deduce that the temperature is expressed by:

$$T(t,\mathbf{x}) = \frac{1}{3k\varrho(t,\mathbf{x})}\int_{\mathbb{R}^3} |\mathbf{v} - \mathbf{u}(t,\mathbf{x})|^2 f(t,\mathbf{x},\mathbf{v})d\mathbf{v},$$

and this yields the Maxwellian distribution $\mathcal{M}(f)$ from (3),

$$\mathcal{M}(f)(t,\mathbf{x},\mathbf{v}) = \frac{\varrho(t,\mathbf{x})}{[2\pi kT(t,\mathbf{x})]^{3/2}} \exp\left(-\frac{|\mathbf{v} - \mathbf{u}(t,\mathbf{x})|^2}{2kT(t,\mathbf{x})}\right).$$

This quantity is denoted by $\mathcal{M}(f)$ because it is the unique Maxwellian distribution which shares all its moments in $\mathbf{v}$ with the ones of the generic kinetic density f.

Because of both its complex integral formulation and its quadratic nonlinearity, the complete Boltzmann collision term is considered difficult to handle in many situations; therefore one is interested in so–called "model equations" which are easier to tackle while sharing some of the essential properties of the original (1). A very classical one is due to Bhatnagar, Gross, Krook and Welander [22] and reads:

$$\partial_t f + \mathbf{v}.\nabla f = \nu(\mathcal{M}(f) - f) := \mathcal{J} f, \qquad \nu \geq 0, \tag{4}$$

where ν is a mean collision frequency related to the inverse Knudsen number and which may be constant or velocity-dependent according to the model. More complex models can be derived following the Gross-Jackson procedure as explained in the Chapter IV of [22]; in general, one asks that:

1. the approximate collision $\mathcal{J}$ term must have the same 5 collision invariants,
2. it has an H-type theorem reflecting its tendency to a Maxwellian distribution.

These two properties are clearly satisfied by the BGK term, $\mathcal{J}(f) := \nu(\mathcal{M}(f) - f)$, despite its nonlinearity in f is worse than the quadratic one of the original collision term. However, despite its simplicity, the BGK relaxation term allows to derive macroscopic balance laws by means of the first order Chapman-Enskog expansion which are identical[3] to the original Boltzmann equation. We now sketch this computation for the simple model (4): by taking moments in $\mathbf{v}$ of (1) or (4)

[2] $k = R$, the gas constant when the particle's mass equals 1.

[3] up to the wrong value of Prandtl's number of 1 against 0.7 for air.

against the 5 collisional invariants, we get the following system:

$$\partial_t \varrho + \nabla.(\varrho \mathbf{u}) = 0,$$
$$\partial_t(\varrho \mathbf{u}_i) + \sum_{j=1}^{3} \partial_{\mathbf{x}_j} \left(\varrho \mathbf{u}_i \mathbf{u}_j + p_{i,j}(t,\mathbf{x}) \right) = 0, \qquad i = 1,2,3,$$
$$\partial_t \left(\frac{1}{2}\varrho |\mathbf{u}|^2 + \varrho\varepsilon \right) + \sum_{i=1}^{3} \partial_{\mathbf{x}_i} \left(\varrho \mathbf{u}_i (\varepsilon + \frac{1}{2}|\mathbf{u}|^2) + \sum_{j=1}^{3} \mathbf{u}_j p_{i,j} \right) = -\sum_{i=1}^{3} \partial_{\mathbf{x}_i} q_i.$$

Two new quantities have been introduced in the preceding expression: the stress tensor and the heat flux, which numerical computation will be scrutinized in the sequel,

$$p_{i,j}(t,\mathbf{x}) = \int_{\mathbb{R}^3} \mathbf{c}_i \mathbf{c}_j f(t,\mathbf{x},\mathbf{v}) d\mathbf{v}, \qquad q_i(t,\mathbf{x}) = \int_{\mathbb{R}^3} \mathbf{c}_i |\mathbf{c}|^2 f(t,\mathbf{x},\mathbf{v}) d\mathbf{v}. \tag{5}$$

We also define the pressure $p(t,\mathbf{x})$ as follows:

$$p(t,\mathbf{x}) = \frac{1}{3} \int_{\mathbb{R}^3} |\mathbf{c}|^2 f(t,\mathbf{x},\mathbf{v}) d\mathbf{v} = \frac{2}{3} \varrho\varepsilon(t,\mathbf{x}).$$

These conservation equations, on the further assumption of an equation of state $\varepsilon = \varepsilon(\varrho, T)$, a constitutive assumption of the viscous stress to the rate of strain,

$$\sigma_{i,j} := p_{i,j} - p\delta_{i,j} = \mu \left(\partial_{\mathbf{x}_j} \mathbf{u}_i + \partial_{\mathbf{x}_i} \mathbf{u}_j \right) + \lambda \delta_{i,j} \partial_{\mathbf{x}_k} \mathbf{u}_k, \qquad \lambda = -\frac{2}{3}\mu,$$

and the heat flux to the temperature gradient, usually taken as Fourier's law $q_i = -\kappa \partial_{\mathbf{x}_i} T$ leads to the compressible Navier-Stokes equations. The Chapman-Enskog approximation of (4) is rather straightforward: is consists in assuming that $\nu \gg 1$ and rewriting the BGK equation under the form,

$$f = \mathcal{M}(f) - \frac{1}{\nu}(\partial_t f - \mathbf{v}.\nabla f) := \mathcal{M}(f) - \frac{1}{\nu}\tilde{f},$$

which yields (following *e.g.* [51], [22] pp. 110-111 and 124 or [44] p.104),

$$\tilde{f} = \frac{1}{T} \left(\frac{|\mathbf{c}|^2}{2kT} - \frac{5}{2} \right) \sum_{i=1}^{3} \mathbf{c}_i \partial_{\mathbf{x}_i} T + \frac{1}{kT} \sum_{i,j=1}^{3} \mathbf{c}_i \mathbf{c}_j \partial_{\mathbf{x}_j} \mathbf{u}_i.$$

Inserting this distribution function into the definitions of the stress tensor and the heat flux, taking again moments in the $\mathbf{v}$ variable and fixing $\nu = p/\mu$ in (4) retrieves the preceding compressible Navier-Stokes equations with:

$$\sigma_{i,j} = \frac{p}{\nu} \left(\partial_{\mathbf{x}_j} \mathbf{u}_i + \partial_{\mathbf{x}_i} \mathbf{u}_j - \frac{2}{3} \delta_{i,j} \partial_{\mathbf{x}_k} \mathbf{u}_k \right), \qquad q_i = -\frac{5}{2} k \frac{p}{\nu} \partial_{\mathbf{x}_i} T.$$

In particular, $\lambda = -\frac{2}{3}\mu$ for this choice. From the point of view of practical computation of macroscopic quantities given by moments of f, it makes therefore sense to devise numerical schemes which simulate the approximate model (4) rather than the complete problem (1) as the consistency with compressible Navier-Stokes equations is likely to be satisfying [22] as soon as parameters are chosen correctly.

1.3. **Scope and outline of the paper.** Our main goal hereafter is to present an original manner to derive so–called "well-balanced" numerical schemes in the sense of [34] for the simplified BGK model (4) of the Boltzmann equation when f depends only on one space variable, that is, $f = f(t, x, \mathbf{v})$ with $x \in \mathbb{R}$, $\mathbf{v} \in \mathbb{R}^3$. This corresponds to a rather realistic modeling of a one-dimensional configuration where particles can still wander with a 3-dimensional peculiar velocity.

In the perspective of numerical schemes, it is fully consistent with the "finite-volumes" discretization of transport equations because in such a method, one is always led to tackle one-dimensional problems in the space variable, that is, in the direction orthogonal to the interface separating 2 adjacent computational cells. We shall therefore study well-balanced discretizations of the initial-boundary problem for the approximate model of the one-dimensional Boltzmann equation [14]:

$$\partial_t f + \xi \partial_x f = \nu(\mathcal{M}(f) - f), \qquad x := \mathbf{x}_1,\ \xi = \mathbf{v}_1.$$

In particular, we shall be especially interested in the accurate computation of perturbations of uniform, steady equilibria $M(\mathbf{v})$ with zero bulk velocity, for which it is reasonable to assume (see *e.g.* [23] p.103):

$$f(t, x, \mathbf{v}) = M(\mathbf{v})[1 + h(t, x, \mathbf{v})].$$

In this case, the perturbation h is meant to satisfy the linearized BGK equation,

$$\partial_t h + \xi \partial_x h = \nu \left(\sum_{i=0}^{4} \int_{\mathbb{R}^3} M(\mathbf{v}')\psi_i(\mathbf{v}')h(t, x, \mathbf{v}')d\mathbf{v}' - h \right) := -\nu(Id - \mathcal{P})h, \tag{6}$$

with ψ_i, $i = 0, ..., 4$ being the orthonormal basis functions of the vector space spanned by the 5 collisional invariants. Their expression is available in several papers [6, 13, 30, 49] and the integral term in (6) is usually written like:

$$\mathcal{P}h(t, x, \mathbf{v}) = \int_{\mathbb{R}^3} M(\mathbf{v}') \left[1 + 2\mathbf{v}.\mathbf{v}' + \frac{2}{3}\left(|\mathbf{v}|^2 - \frac{3}{2}\right)\left(|\mathbf{v}'|^2 - \frac{3}{2}\right) \right] h(t, x, \mathbf{v}')d\mathbf{v}'.$$

This is the kind of integro-differential equation to which it becomes possible to apply the well-balanced strategy presented in [31] (which generalized [32, 33]) at the price, however, of a higher computational complexity. In order to balance accurately the convection and the collision processes in (6), it is necessary not to dissociate them as it is nearly always done usually in the time-splitting method [29, 52, 53, 54]. One has therefore to include the collision term's effects inside the numerical fluxes at each interface; this can be achieved by means of a formal localization involving Dirac masses (such a process can sometimes be proved rigorously: see §2 in [33]),

$$\partial_t h + \xi \partial_x h = -\nu \Delta x \sum_{j \in \mathbb{Z}} (Id - \mathcal{P})h\ \delta\left(x - (j - \frac{1}{2})\Delta x\right), \tag{7}$$

where $\Delta x > 0$ is the space-step of the chosen computational grid. When deriving any finite volume scheme for (7), it is necessary to compute numerical fluxes at each interface $(j - \frac{1}{2})\Delta x$, $j \in \mathbb{Z}$: it is precisely at these locations that the collision term is "ignited". When h is discontinuous, the right-hand side of (7) contains a so–called "non-conservative product" [48]: in order to define correctly such a quantity in this context, it is necessary to resolve the steady-state problem for (6).

It is at this level that a remarkable observation originally due to Case for radiative transfer problems [15, 16], but extended to linearized models of the Boltzmann equation by Cercignani and collaborators (see chapter VII in [22] and also [2, 17, 18, 19, 20, 21, 24]) enters the picture: the complexity of solving of the steady-state problem for (6) can be strongly reduced by applying an astute decomposition of the unknown $\bar{h}(x, \mathbf{v})$. This brilliant idea will be presented in some detail in our §2 in the context of the time-dependent problem (6) with $\nu = 1$. Especially, the stationary equation can be split in such a way that the shear effects and the heat transfer decouple: the corresponding scalar "reduced viscosity equation" (according to the terminology of [17]) will be derived in §2.2 and the 2×2 system for heat transfer effects, in §2.3 (some complementary details concerning the heat transfer system are developed in Appendix A). In §2.4, consistency with compressible Navier-Stokes equations is studied. In §3, the numerical aspects of such a strategy will be examined in detail: basically, one starts in §3.1 by setting up a Gaussian quadrature in the ξ variable. Then [31] can be partly followed in order to treat the reduced viscosity equation: see §3.2. More involved numerical techniques are necessary for treating the system rendering the heat transfer effects: see §3.3. In §3.4, we shall explain some links existing with the so–called "micro-macro decomposition" [49, 50] of the Boltzmann equation. Numerical results on a standard transient Couette flow problem are displayed in §4 with several values of the accommodation coefficient at the boundaries. Some components of the stress tensor must be constant at the numerical steady-state according to *e.g.* [70]: it can be checked on Figs. 6 and 8 that our well-balanced approach behaves much better than the usual time-splitting scheme on this particular point. A similar presentation appears also in §5 for heat transfer problems partly taken from [60] and a sound wave propagation taken from [65]: here again, some quantities are meant to be constant at numerical steady state, namely the momentum and the heat flow as shown on Figs. 11 and 13. A question of interest is the behavior of the numerical scheme for small Knudsen numbers, that is, for values of $\nu \gg 1$ in (6). It turns out, and we shall show numerically in §6 that our well-balanced strategy is completely independent of the size of ν. In particular, only a tiny modification, already explained in §3.3 of the former paper [31], allows to handle stiff problems endowed with a small Knudsen number. A preliminary numerical experiment involving a computational domain split into several regions, each one being endowed with a different mean free path with discontinuous borders, is presented in §6.2. Finally, some concluding remarks are drawn in section 7.

2. **Elementary solutions for the BGK model of Boltzmann equation.**

2.1. **Cercignani's decomposition of a time-dependent problem.** Here, we mean to follow both [22], Chapter VII, and [45, 65, 62] in order to present the decomposition of $h(t, x, \mathbf{v})$ leading to the aforementioned decoupling properties. We start from the linearized equation (6), change its variables,

$$\nu\sqrt{\frac{1}{2kT_0}}x \to x, \qquad \nu t \to t, \qquad \sqrt{\frac{1}{2kT_0}}\mathbf{v} \to \mathbf{v},$$

where $T_0 > 0$ is a temperature of reference and define the 5-components vector:

$$\Phi(\mathbf{v}) = \frac{1}{\pi^{\frac{3}{4}}}\begin{pmatrix} 1 & \sqrt{\frac{2}{3}}(|\mathbf{v}|^2 - \frac{3}{2}) & \sqrt{2}\mathbf{v}_2 & \sqrt{2}\mathbf{v}_3 & \sqrt{2}\mathbf{v}_1 \end{pmatrix}^T. \tag{8}$$

A direct computation shows that: (^{T} denotes transposition)

$$\mathcal{P}h(t, x, \mathbf{v}) = \int_{\mathbb{R}^3} M(\mathbf{v}') \left[\Phi(\mathbf{v})^T \Phi(\mathbf{v}')\right] h(t, x, \mathbf{v}')d\mathbf{v}'.$$

Moreover, there holds an orthogonality property:

$$\forall i,j \in \{0,1,2,3,4\}^2, \qquad \int_{\mathbb{R}^3} \Phi(\mathbf{v})_i \Phi(\mathbf{v})_j \exp(-|\mathbf{v}|^2) d\mathbf{v} = \delta_{i,j}.$$

Following Cercignani [22], we introduce the (normalized) functions:

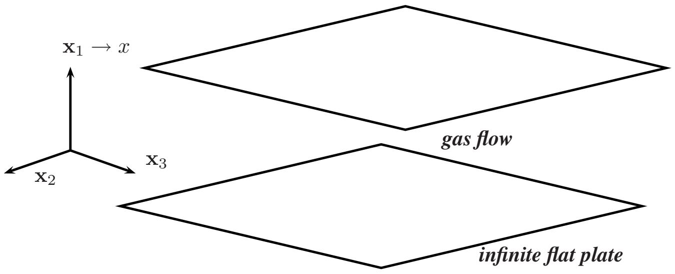

FIGURE 1. Geometry of the one-dimensional model (6).

$$\mathbf{G}(\mathbf{v}_2,\mathbf{v}_3) = \begin{pmatrix} g_1(\mathbf{v}_2,\mathbf{v}_3) \\ g_2(\mathbf{v}_2,\mathbf{v}_3) \\ g_3(\mathbf{v}_2,\mathbf{v}_3) \\ g_4(\mathbf{v}_2,\mathbf{v}_3) \end{pmatrix} = \frac{1}{\sqrt{\pi}} \begin{pmatrix} 1 \\ (\mathbf{v}_2^2 + \mathbf{v}_3^2 - 1) \\ \sqrt{2}\mathbf{v}_2 \\ \sqrt{2}\mathbf{v}_3 \end{pmatrix}, \tag{9}$$

which are orthogonal in the following sense,

$$\forall i,j \in \{1,2,3,4\}^2, \qquad \int_{\mathbb{R}^2} g_i(\mathbf{v}_2,\mathbf{v}_3) g_j(\mathbf{v}_2,\mathbf{v}_3) \exp(-\mathbf{v}_2^2 - \mathbf{v}_3^2) d\mathbf{v}_2 d\mathbf{v}_3 = \delta_{i,j}.$$

Recalling the notation $\mathbf{v}_1 = \xi$, the solution $h(t,x,\mathbf{v})$ of (6) can be expanded:

$$h(t,x,\mathbf{v}) = \sum_{i=1}^{4} \Psi_i(t,x,\xi) g_i(\mathbf{v}_2,\mathbf{v}_3) + \Psi_5(t,x,\mathbf{v}), \tag{10}$$

where the components Ψ_i are "unusual moments" of h and read for $i = 1,2,3,4$,

$$\Psi_i(t,x,\xi) = \int_{\mathbb{R}^2} h(t,x,\mathbf{v}_1,\mathbf{v}_2,\mathbf{v}_3) g_i(\mathbf{v}_2,\mathbf{v}_3) \exp(-\mathbf{v}_2^2 - \mathbf{v}_3^2) d\mathbf{v}_2 d\mathbf{v}_3 \tag{11}$$

and Ψ_5 belongs to the orthogonal complement of the subspace spanned by the g_i's in the weighted Hilbert space $L^2(\mathbb{R}^3, \exp(-|\mathbf{v}|^2)d\mathbf{v})$. It turns out that each component $\Psi_i(t,x,\xi)$ is closely related to the perturbations in ϱ, T, and the fluid's transverse velocities $\mathbf{u}_2$ and $\mathbf{u}_3$, respectively. All in all, the equation (6) for $h(t,x,\mathbf{v})$ rewrites:

$$\partial_t \Psi + \xi \partial_x \Psi = \left(\int_{\mathbb{R}} [\mathbf{P}(\xi)\mathbf{P}(\xi')^T + \mathbf{Q}(\xi)\mathbf{Q}(\xi')^T] \Psi(t,x,\xi') \frac{\exp(-|\xi'|^2)}{\sqrt{\pi}} d\xi' \right) - \Psi, \tag{12}$$

with $\Psi(t,x,\xi)$ being the vector of 4 components and $\mathbf{P}, \mathbf{Q}$ the two matrices,

$$\mathbf{P}(\xi) = \begin{pmatrix} \sqrt{\frac{2}{3}}(\xi^2 - \frac{1}{2}) & 1 & 0 & 0 \\ \sqrt{\frac{2}{3}} & 0 & 0 & 0 \\ 0 & 0 & 1 & 0 \\ 0 & 0 & 0 & 1 \end{pmatrix}, \qquad \mathbf{Q}(\xi) = \sqrt{2}\xi \begin{pmatrix} 1 & 0 & 0 & 0 \\ 0 & 0 & 0 & 0 \\ 0 & 0 & 0 & 0 \\ 0 & 0 & 0 & 0 \end{pmatrix}. \tag{13}$$

Cercignani [23] (page 112) claims that Ψ_5, solution of

$$\partial_t \Psi_5 + \xi \partial_x \Psi_5 + \Psi_5 = 0,$$

plays little, if any, role. Hence Ψ_1, Ψ_2, which are responsible for perturbations of density and temperature, satisfy a 2×2 system of integro-diffenrential equations whereas Ψ_3 and Ψ_4, describing fluctuations of the transverse momenta, are solutions of a scalar problem that Cercignani refers to as the "reduced viscosity equation".

2.2. **Elementary solutions of the "reduced viscosity equation".** In order to treat this scalar equation, we introduce a simpler notation $\psi(t, x, \xi)$ which will stand for either Ψ_3 or Ψ_4 according to the context and be solution of an intial/boundary value problem for the following scalar equation:

$$\partial_t \psi + \xi \partial_x \psi = \int_{\mathbb{R}} \psi(t, x, \xi') \frac{\exp(-|\xi'|^2)}{\sqrt{\pi}} d\xi' - \psi, \tag{14}$$

which corresponds to one of the last 2 lines of (12)–(13). As it is customary for well-balanced schemes, we are primarily interested in solving the stationary equation. It has been first derived in [17] where the steady-state boundary problem has been studied; later, several existence, uniqueness and stability results have been produced in [18, 40, 11, 41, 42, 3, 67]. More precisely, according to [11] (pp.18-19), the so–called "forward-backward problem" for the equation,

$$\xi \partial_x \psi = \int_{\mathbb{R}} \psi(x, \xi') \frac{\exp(-|\xi'|^2)}{\sqrt{\pi}} d\xi' - \psi, \qquad x \in (-a, a), \tag{15}$$

with inflow boundary conditions in $x = \pm a$,

$$\psi(\pm a, \mp|\xi|) = g(\mp|\xi|), \qquad g \in L^2\left(\mathbb{R}, \exp(-|\xi|^2)d\xi\right),$$

has a unique solution $\psi \in C^0(-a, a; L^2(\mathbb{R}, \exp(-|\xi|^2)d\xi))$, see also [3, 35, 39, 67, 68]. Moreover, a useful feature of this stationary problem is that its solution admits an explicit formulation which is found by separating the variables. Following [17] (see also [15, 16, 7, 64] for similar matters in radiative transfer theory), we assume that:

$$\psi(x, \xi) = \exp(-x/\nu)\varphi_\nu(\xi),$$

with $\nu \in \mathbb{R}$ being usually called the "constant of separation". By inserting this *ansätze* in the equation, one sees that φ_ν must satisfy:

$$\left(1 - \frac{\xi}{\nu}\right) \varphi_\nu(\xi) = \int_{\mathbb{R}} \varphi_\nu(\xi') \frac{\exp(-|\xi'|^2)}{\sqrt{\pi}} d\xi', \tag{16}$$

with the right-hand side which value can be normalized to unity by linearity. One has therefore to distinguish between the values for which $\nu - \xi$ can vanish or not; thus φ_ν is a distribution including a Cauchy principal value denoted by PV,

$$\varphi_\nu(\xi) = PV \frac{1}{1 - \xi/\nu} + p(\nu)\delta(\nu - \xi), \tag{17}$$

where the weight of the Dirac mass reads:

$$p(\nu) = PV \int_{\mathbb{R}} \frac{\exp(\nu^2 - \xi^2)}{1 - \nu/\xi} d\xi = \sqrt{\pi}\left(\exp(\nu^2) - 2\nu \int_0^\nu \exp(t^2)dt\right). \tag{18}$$

The linear problem (16) can be recast in the general theory of integral equations of the third kind [8]; indeed, Theorem 3 of [8] applies with the notation,

$$(\nu - t)\varphi_\nu(t) = \nu \int K(t')\varphi_\nu(t')dt', \quad g(t) = \nu - t, \; K(t) = \frac{\exp(-t^2)}{\sqrt{\pi}}, \; f \equiv 0.$$

The solution (17)–(18) is derived in [22] (pp.158/159): however, it corresponds to a particular case of the general formula (3.15) in [8] with the choices:

$$n = 1,\ x(t) \equiv 1,\ p_1(t) = \frac{tK(t)}{\nu K(\nu)} = \frac{\exp(\nu^2 - t^2)}{1 - t/\nu},\ g(t) = 1 - \frac{t}{\nu}.$$

The singular functions φ_ν constitute a set of "generalized eigenfunctions" endowed with specific orthogonality and completeness properties (see [22] pp.158-159 or [16, 41, 42, 43]). As a consequence, it comes that any smooth solution of the stationary problem for (14) with inflow boundary conditions can be expressed as follows:

$$\psi(x, \xi) = \alpha + \beta(x - \xi) + \int_{\mathbb{R}} A(\nu) \exp(-x/\nu)\varphi_\nu(\xi) d\nu. \tag{19}$$

The quantities α, β and $A(\nu)$ are determined by the boundary conditions in $x = \pm a$.

Remark 1. Because of the very definition of ψ given by,

$$\psi(t, x, \xi = \mathbf{v}_1) = \sqrt{\frac{2}{\pi}} \int_{\mathbb{R}^2} \mathbf{v}_j h(t, x, \mathbf{v}) \exp(-\mathbf{v}_2^2 - \mathbf{v}_3^2) d\mathbf{v}_2 d\mathbf{v}_3,$$

for $j = 2$ or 3, its average yields the fluctuations of the transverse momentum:

$$\int_{\mathbb{R}} \psi(t, x, \xi) \frac{\exp(-|\xi|^2)}{\pi\sqrt{2}} d\xi = \varrho \mathbf{u}_j(t, x). \tag{20}$$

The proof is straightforward: one starts from the expansion (10), and writes the definition of the macroscopic momentum as a function of the kinetic distribution h,

$$\varrho \mathbf{u}_j(t, x) = \int_{\mathbb{R}} \frac{\exp(-|\mathbf{v}_1|^2)}{\sqrt{\pi}} \left(\int_{\mathbb{R}^2} \mathbf{v}_j h(t, x, \mathbf{v}) \frac{\exp(-\mathbf{v}_2^2 - \mathbf{v}_3^2)}{\pi} d\mathbf{v}_2 d\mathbf{v}_3 \right) d\mathbf{v}_1.$$

Thanks to the orthogonality property of the functions $g_i(\mathbf{v}_2, \mathbf{v}_3)$ with respect to the $\exp(-\mathbf{v}_2^2 - \mathbf{v}_3^2)$-weighted scalar product, one can deduce that for $j = 2$ or 3,

$$\varrho \mathbf{u}_j(t, x) = \int_{\mathbb{R}} \frac{\exp(-|\xi|^2)}{\sqrt{\pi}} \Psi_{j+1}(t, x, \xi) \frac{d\xi}{\sqrt{2\pi}} = \frac{1}{\pi\sqrt{2}} \int_{\mathbb{R}} \exp(-|\xi|^2) \Psi_{j+1}(t, x, \xi) d\xi.$$

2.3. **Elementary solutions of the heat transfer system.** In this subsection, we focus on the 2×2 coupled system which corresponds to the 2 first lines of (12)–(13) and work hereafter with the following notation:

$$\mathbb{R}^2 \ni \Psi(t, x, \xi) := (\Psi_1\ \Psi_2)^T.$$

Here again, we are mainly interested in the solution $\Psi(x, \xi)$ of the stationary boundary-value problem which reads:

$$\xi \partial_x \Psi = \left(\int_{\mathbb{R}} [\mathbf{P}(\xi)\mathbf{P}(\xi')^T + 2\xi\xi' \begin{pmatrix} 1 & 0 \\ 0 & 0 \end{pmatrix}] \Psi(x, \xi') \frac{\exp(-|\xi'|^2)}{\sqrt{\pi}} d\xi' \right) - \Psi,$$

with the truncated matrix $\mathbf{P}$,

$$\mathbf{P}(\xi) = \begin{pmatrix} \sqrt{\frac{2}{3}}(\xi^2 - \frac{1}{2}) & 1 \\ \sqrt{\frac{2}{3}} & 0 \end{pmatrix},$$

and some smooth inflow boundary conditions in $x = \pm a$ like in the preceding subsection. Let us first observe that the vector-valued integral,

$$\begin{pmatrix} 1 & 0 \\ 0 & 0 \end{pmatrix} \int_{\mathbb{R}} \xi' \Psi(x, \xi') \frac{\exp(-|\xi'|^2)}{\sqrt{\pi}} d\xi', \tag{21}$$

doesn't depend on x and is just a constant (the mass flow rate). Hence, according to [59, 45] (or [22] page 156), it can be safely removed (see details in our Appendix A). The main result of [45] (see also [61, 62, 63]) states that the solution of:

$$\xi\partial_x\Psi = \mathbf{P}(\xi)\left(\int_{\mathbb{R}} \mathbf{P}(\xi')^T\Psi(x,\xi')\frac{\exp(-|\xi'|^2)}{\sqrt{\pi}}d\xi'\right) - \Psi, \qquad x\in(-a,a), \tag{22}$$

can be written as,

$$\Psi(x,\xi) = \sum_{i=1}^{2}\mathbf{P}(\xi)[\alpha_i+\beta_i(x-\xi)]\vec{e}_i + \int_{\mathbb{R}} A_i(\nu)\Phi_i(\nu,\xi)\exp(-x/\nu)d\nu, \tag{23}$$

where we have set

$$\vec{e}_1 = (1\ 0)^T, \qquad \vec{e}_2 = (0\ 1)^T.$$

The singular functions $\Phi(\nu,\xi)\in\mathbb{R}^2$ are the analogues of the (scalar) generalized eigenfunctions $\varphi_\nu(\xi)$ in the preceding subsection; they satisfy the equation,

$$\Phi_i(\nu,\xi) = \frac{1}{\sqrt{\pi}}\left(PV\frac{1}{1-\nu/\xi} + p_i(\nu)\delta(\nu-\xi)\right)\mathbf{P}(\xi)\mathbf{R}_i(\nu), \tag{24}$$

where, for $\mathbf{S}(\nu) := \mathbf{P}(\nu)^T\mathbf{P}(\nu)\frac{\exp(-|\nu|^2)}{\sqrt{\pi}}$ and Id standing for the identity matrix,

$$\left[Id - PV\left(\int_{\mathbb{R}}\mathbf{S}(\xi')\frac{d\xi'}{1-\nu/\xi'}\right) - p(\nu)\mathbf{S}(\nu)\right]\mathbf{R}(\nu) = 0. \tag{25}$$

The constants of separation are the zeros of the "dispersion relation":

$$\Lambda(z) = \left|Id - \int_{\mathbb{R}}\mathbf{S}(\xi)\frac{d\xi}{1-\xi/z}\right|. \tag{26}$$

Theorem 1 in [45] ensures that the set of functions $\mathbf{P}(\xi)\vec{e}_i$, $\mathbf{P}(\xi)(x-\xi)\vec{e}_i$ and $\Phi_i(\nu,\xi)$ for $i=1,2$ and $\xi\in\mathbb{R}$ constitutes a complete basis set for smooth solutions of (22).

Remark 2. Again, by the very definition of $\Psi(t,x,\xi)$ given by,

$$\Psi(t,x,\xi) = \frac{1}{\sqrt{\pi}}\int_{\mathbb{R}^2}\begin{pmatrix}1\\ \mathbf{v}_2^2+\mathbf{v}_3^2-1\end{pmatrix}h(t,x,\mathbf{v})\exp(-\mathbf{v}_2^2-\mathbf{v}_3^2)d\mathbf{v}_2d\mathbf{v}_3,$$

its averages yield the fluctuations of the density and the temperature of the gas:

$$\int_{\mathbb{R}}\begin{pmatrix}1 & 0\\ \frac{2}{3}(\xi^2-\frac{1}{2}) & \frac{2}{3}\end{pmatrix}\Psi(t,x,\xi)\frac{\exp(-|\xi|^2)}{\pi}d\xi = \begin{pmatrix}\varrho(t,x)\\ T(t,x)\end{pmatrix}. \tag{27}$$

Other quantities, like the heat flow or the pressure, can be deduced as well [65].

2.4. **Consistency with Navier-Stokes-Fourier equations.** On pages 106–108 in [23], Cercignani explains that stationary solutions $\bar{h}$ to the linearized Boltzmann equation (2) depending only on one space variable x are naturally consistent with the compressible Navier-Stokes equations linearized around $\varrho_0, \mathbf{u}\equiv 0, T=T_0$. Here, we want to show that h, as reconstructed by (10) from the explicit solutions computed in (19) and (23), enters his framework and is therefore consistent with the linearized compressible Navier-Stokes system extracted from the Chapman-Enskog expansion for the BGK model (see [51]). Recalling the collisional invariants $\Phi(\mathbf{v})$ in (8), one can write down the linearized BGK collision operator as follows:

$$L_{BGK}(h)(x,\mathbf{v}) = \sum_{i=1}^{5}\left(\int M(\mathbf{v}')\Phi_i(\mathbf{v}')h(x,\mathbf{v}')d\mathbf{v}'\right)\Phi_i(\mathbf{v}) - h(x,\mathbf{v}).$$

Thus, mimicking the computations in [23], one can invert easily the linear equation $L_{BGK}(h) = \mathbf{v}_1 \Phi_i$ and the corresponding solution reads:

$$h(x, \mathbf{v}) = \left[\sum_{i=1}^{5} \left(\int M(\mathbf{v}')\Phi_i(\mathbf{v}')h(x, \mathbf{v}')d\mathbf{v}' \right) - \mathbf{v}_1 \right] \Phi_i(\mathbf{v}).$$

Hence the expansion written on page 106 in [23] rewrites for the present BGK model:

$$h(c, \mathbf{v}) = \sum_{i=1}^{5} A_i \Phi_i(\mathbf{v}) + \sum_{i=1}^{4} B_i \Phi_i(\mathbf{v})(x - \mathbf{v}_1) + \int_{\mathbb{R}} A(\nu) \exp(-x/\nu) \tilde{\varphi}_\nu(\mathbf{v}) d\nu, \quad (28)$$

where some terms generated by $L_{BGK}^{-1}(\mathbf{v}_1 \Phi_i)$, $i \in \{1, 2, 3, 4\}$, have been included in the A_i coefficients. For instance, by picking up $\Psi_3(x, \mathbf{v}_1) = \psi(x, \xi)$, one sees that the expression (19) has to be multiplied by $g_3(\mathbf{v}_2, \mathbf{v}_3) = \sqrt{\frac{2}{\pi}} \mathbf{v}_2$ and this matches one part of the equation (28). The remaining part, besides Ψ_5 which can be put inside the integral sign and Ψ_4 which is very similar to Ψ_3, concerns Ψ_2 which can also be included in (28) at the price of slightly heavier computations.

By definition, the expression (23) of $\Psi(x, \xi) \in \mathbb{R}^2$ free from damped modes reads:

$$\Psi(x, \xi) = \begin{pmatrix} \alpha_1 \sqrt{\frac{2}{3}}(\xi^2 - \frac{1}{2}) + \alpha_2 + (x - \xi) \left(\beta_1 \sqrt{\frac{2}{3}}(\xi^2 - \frac{1}{2}) + \beta_2 \right) \\ \sqrt{\frac{2}{3}}(\alpha_1 + \beta_1(x - \xi)) \end{pmatrix}.$$

This yields that, upon neglecting both exponentially damped terms and the contributions of $\Psi_{3,4,5}$, the kinetic density $h(x, \mathbf{v})$ can be reconstructed as follows:

$$\begin{aligned} \sqrt{\pi} h(x, \mathbf{v}) &= \Psi(x, \xi). \big(g_1(\mathbf{v}_2, \mathbf{v}_3) \ g_2(\mathbf{v}_2, \mathbf{v}_3) \big)^T \\ &= \sqrt{\tfrac{2}{3}} \alpha_1 (\xi^2 - \tfrac{3}{2}) + \alpha_2 + (x - \xi) \left[\beta_1 \sqrt{\tfrac{2}{3}} (\xi^2 - \tfrac{3}{2}) + \beta_2 \right] \\ &\qquad + \sqrt{\tfrac{2}{3}} [\alpha_1 + \beta_1 (x - \xi)] (\mathbf{v}_2^2 + \mathbf{v}_3^2) \\ &= \alpha_1 \Phi_2(\mathbf{v}) + \beta_1 (x - \xi) \Phi_2(\mathbf{v}) + \alpha_2 \Phi_1(\mathbf{v}) + \beta_2 (x - \xi) \Phi_1(\mathbf{v}). \end{aligned}$$

The last equality results from the simple observation that as $\xi = \mathbf{v}_1$, there holds:

$$\sqrt{\frac{2}{3}} \left(\xi^2 - \frac{3}{2} + \mathbf{v}_2^2 + \mathbf{v}_3^2 \right) = \sqrt{\pi} \Phi_2(\mathbf{v}).$$

At this point, since we have fully shown that the expansion (10) can be put under the form (28), we are in position to take advantage of the conclusions drawn by Cercignani in [23], page 108. Namely, by dropping the terms weighted by exponential terms, we get that the corresponding macroscopic quantities $\varrho(t, x)$, $\mathbf{u}(t, x)$, $T(t, x)$ satisfy the Navier-Stokes-Fourier equations linearized around the basic values $\varrho_0 > 0$, $\mathbf{u} \equiv 0$ and $T = T_0 > 0$. The expression of the viscosity and heat-conduction coefficients μ and κ involves the one of L_{BGK}^{-1}: hence they depend on the particular kinetic model under consideration. In our case, it implies that the underlying Navier-Stokes system will involve an incorrect Prandtl number.

3. **Well-balanced and Analytical Discrete-Ordinate (ADO) method.** Hereafter we work with a uniform Cartesian computational grid in space and time determined by $\Delta x > 0$ and $\Delta t > 0$ where the time step is meant to satisfy the standard hyperbolic CFL condition, $\max(|\xi|)\Delta t \leq \Delta x$ such that $\Psi(t, x, \xi) > 0$. The well-balanced character of our scheme will come as a consequence of discretizing the "localized equation" (7). Similar methodology has already been used for radiative transfer problems in [31] and earlier, for discrete-velocity models, in [32, 33].

3.1. **Gaussian quadrature in the velocity variable and ADO.** The Case's method of elementary functions has been extended by many authors, see *e.g.* [16, 17, 18, 22, 25, 26, 43]. For numerical purposes, it has been introduced under the name "Analytical Discrete-Ordinate method" in [7]. Roughly speaking, it consists in first, introducing a N-point Gaussian quadrature on the interval[4] $(0,1)$ given by the following points and weights:

$$\boldsymbol{\xi} = (\xi_1, \xi_2, ..., \xi_N) \in (0,1)^N, \qquad \boldsymbol{\omega} = (\omega_1, ..., \omega_N) \in \mathbb{R}^+.$$

This quadrature is multiplied by a number $\xi_{max} \simeq \max(|\xi|)$ which is an estimate of the maximal velocity that particles may have, that is, for which $\Psi(t, x, \xi_{max}) > 0$ at some location $t, x \in \mathbb{R}_+ \times \mathbb{R}$. Hence the parameters are modified accordingly:

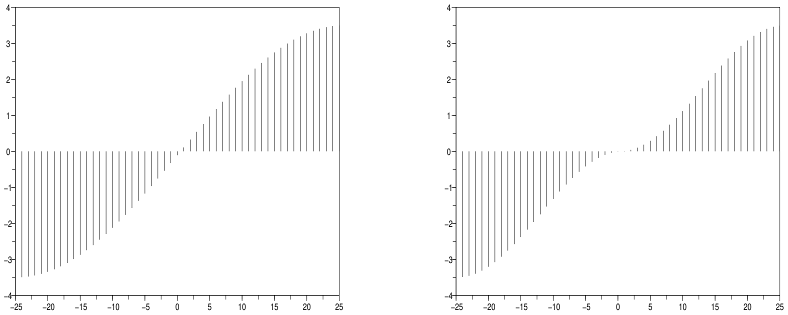

FIGURE 2. Standard 50-points Gaussian quadrature rule (left) compared to (29) with $N = 25$ (right) for griding $\xi \in (-3.5, 3.5)$.

$$\boldsymbol{\xi} = \xi_{max}(\xi_1, \xi_2, ..., \xi_N), \qquad \boldsymbol{\omega} = \xi_{max}(\omega_1, ..., \omega_N). \tag{29}$$

From Fig.2, one sees that the choice (29) produces more points near $\xi = 0$, which may improve the overall accuracy of the Gaussian integrals yielding macroscopic moments. Second, it computes a finite set of constants of separation $\boldsymbol{\nu} \in (\mathbb{R}^+)^N$ which is an approximation of both the discrete and continuous part of the spectrum derived in §2.2. Third, it determines the coefficients of the generalized eigenfunctions out of the given inflow boundary conditions. Let us rewrite (15) as follows:

$$\xi \partial_x \psi(x,\xi) + \psi(x,\xi) = \int_0^\infty [\psi(x,\xi') + \psi(x,-\xi')] \frac{\exp(-|\xi'|^2)}{\sqrt{\pi}} d\xi', \quad x \in (-a,a), \tag{30}$$

with $a \in \mathbb{R}$, $\xi \in \mathbb{R}$ and supplemented by inflow boundary conditions:

$$\psi(\pm a, \mp|\xi|) = g(\mp|\xi|), \qquad \xi \in (0, +\infty). \tag{31}$$

Analogously with the continuous case, the separation variable ν is introduced:

$$\psi(x,\xi) = \varphi(\nu,\xi) \exp(-x/\nu).$$

Plugging into (30) and taking the quadrature rule into account yields:

$$\left(1 \mp \frac{\xi_k}{\nu_k}\right) \varphi(\nu, \pm\xi_k) = \sum_{\ell=1}^N \omega_\ell \Big(\varphi(\nu,\xi_\ell) + \varphi(\nu,-\xi_\ell)\Big) \frac{\exp(-\xi_\ell^2)}{\sqrt{\pi}}, \quad k \in \{1, ..., N\}.$$

[4]0 is excluded.

It is at this level that a trick is used in order to reduce the cost of this eigenvalue problem: let us denote $\Phi_\pm(\nu) = (\varphi(\nu, \pm\xi_k))_{k\in\{1,\dots,N\}}$ and Id the identity matrix of $\mathbb{R}^N$. By using the same notation for a vector in $\mathbb{R}^N$ and its corresponding $N \times N$ diagonal matrix, it comes for any ν:

$$\pm\frac{1}{\nu}\boldsymbol{\xi}\Phi_\pm(\nu) = \left(Id - \frac{\boldsymbol{\omega}.\exp(-\boldsymbol{\xi}^2)}{\sqrt{\pi}}\right)\Phi_\pm(\nu) - \frac{\boldsymbol{\omega}.\exp(-\boldsymbol{\xi}^2)}{\sqrt{\pi}}\Phi_\mp(\nu). \tag{32}$$

Barichello, Siewert and Wright [7, 64] now observe that (32) reduces to:

$$\boldsymbol{\xi}^{-1}\left(Id - \frac{2\boldsymbol{\omega}.\exp(-\boldsymbol{\xi}^2)}{\sqrt{\pi}}\right)\boldsymbol{\xi}^{-1}[\Phi_+(\nu) + \Phi_-(\nu)] = \frac{1}{\nu^2}\boldsymbol{\xi}[\Phi_+(\nu) + \Phi_-(\nu)].$$

This problem can be recast under a very tractable one. Indeed, one multiplies on the left by the diagonal $N \times N$ matrix $diag(\sqrt{\omega_k \exp(-\xi_k^2)})$ and obtains:

$$(\boldsymbol{\xi}^{-2} - 2zz^T)X(\nu) = \frac{1}{\nu^2}X(\nu), \qquad z = diag\left(\frac{\sqrt{\omega_k \exp(-\xi_k^2)}}{\pi^{\frac{1}{4}}\xi_k}\right). \tag{33}$$

The eigenvalue problem $\underline{\text{for } \boldsymbol{\nu} \text{ only}}$ is endowed with "good properties" [64]; in particular, as the components of z never vanish, we have the interlacing repartition,

$$0 < \xi_1 < \nu_1 < \xi_2 < \nu_2 < \dots < \xi_N < \nu_N \notin (0, \xi_{max}].$$

Clearly, ν_N stand for the discrete part of the spectrum thus we have a degeneracy at infinity [68] and the corresponding eigenvalues $\pm\nu_N$ are meaningless.

3.2. **Complete time-dependent scheme for shear flow.** We now define a space/time computational grid determined by a time step $\Delta t > 0$ and the uniform width of the cells $\Delta x > 0$ such that the CFL condition holds, $\xi_{max}\Delta t \le \Delta x$:

$$x_j = j\Delta x,\ t^n = n\Delta t,\ C_j = (x_{j-\frac{1}{2}}, x_{j+\frac{1}{2}}), \qquad j \in \mathbb{Z}, n \in \mathbb{N}. \tag{34}$$

Then we introduce approximate values as follows:

$$\psi_j^n(\pm\xi_k) \simeq \psi(t^n, x_j, \pm\xi_k),$$

where ξ_k still refers to the Gaussian quadrature rule (29). The general methodology of well-balanced schemes stems on localizing the source terms of hyperbolic equations onto a discrete lattice; presently, it consists in passing from (14) to:

$$\partial_t\psi + \xi\partial_x\psi = \sum_{j\in\mathbb{Z}}\Delta x\left(\int_{\mathbb{R}}\psi(t,x,\xi')\frac{\exp(-|\xi'|^2)}{\sqrt{\pi}}d\xi' - \psi\right)\delta(x - x_{j+\frac{1}{2}}). \tag{35}$$

Consistency with the continuous problem (14) is a consequence of:

$$\Delta x\sum_{j\in\mathbb{Z}}\delta(x - x_{j+\frac{1}{2}}) \rightharpoonup 1, \qquad \Delta x \to 0.$$

More details about consistency for hyperbolic systems of balance laws are to be found in [1]. For discontinuous solutions, the right-hand side of (35) becomes a non-conservative (NC) product and should be defined carefully. It has been rigorously shown in [33] (see §2.1) that in the simpler case of a discrete velocity model, the localization process yields a BV-bound on the corresponding sequence of solutions. The NC product can therefore be defined as a weak limit in the theory of [48]. It induces a stationary contact discontinuity across which holds a jump relation following the integral curves of the steady-state equation (15): this is the reason why the steady-state problem has been studied in the preceding section. Based on the definition of ψ and fixing the transverse direction to be $\mathbf{x}_3$, the following macroscopic quantities can be recovered according to the quadrature rule (29):

$$\begin{cases} (\varrho\mathbf{u}_3)_j^n = \sum_{k=1}^{N} \omega_k \left[\psi_j^n(\xi_k) + \psi_j^n(-\xi_k)\right] \dfrac{\exp(-\xi_k^2)}{\pi\sqrt{2}} \simeq \varrho\mathbf{u}_3(t^n, x_j, ., .), \\ (p_{1,3})_j^n = \sum_{k=1}^{N} \omega_k \xi_k \left[\psi_j^n(\xi_k) - \psi_j^n(-\xi_k)\right] \exp(-\xi_k^2) \simeq p_{1,3}(t^n, x_j, ., .), \end{cases} \tag{36}$$

i.e. the transverse momentum and the shear stress, respectively (see *e.g.* [6, 70]).

When the ξ-variable is discretized, the kinetic equation (35) becomes a strictly hyperbolic semi-linear system of balance laws [4] which right-hand side contains non-conservative products having an effect only on the lattice $x_{j+\frac{1}{2}}$, $j \in \mathbb{Z}$. In order to be fully consistent with steady-states regimes (which are of particular importance in this context), we choose to apply the Godunov scheme to approximate (35). In the terminology of [1], we thus have Riemann problems containing "zero-waves" at every interface $x_{j+\frac{1}{2}}$ separating two adjacent computational cells C_j and C_{j+1}, see Fig. 3. As done in [1, 31], we first focus on approximately solving the boundary value problem for the steady-state equations (15) assuming that the constants of separation $\boldsymbol{\nu}$ have been computed previously as a pre-processing step.

So let us consider some interface at $x_{j+\frac{1}{2}}$ at time $t^n = n\Delta t$ separating the cells C_j, where the piecewise constant approximation of ψ reads $\psi_j^n(\pm\xi_k)$ and C_{j+1}, where it is $\psi_{j+1}^n(\pm\xi_k)$. The method of elementary solutions for (15) suggests to seek an approximation of (19) under the following form, for $x \in [0, \Delta x]$:

$$\forall k \in \{1, ..., N\}, \qquad \psi(x, \pm\xi_k) \simeq \alpha + \beta(x \mp \xi_k) + E(x, \pm\xi_k, \boldsymbol{\nu}),$$

where E stand for the finite superposition of the damped modes,

$$E(x, \xi, \boldsymbol{\nu}) = \sum_{\ell=1}^{N-1} \left(\frac{A_\ell}{1 - \xi/\nu_\ell} \exp(-x/\nu_\ell) + \frac{B_\ell}{1 + \xi/\nu_\ell} \exp(x/\nu_\ell) \right), \tag{37}$$

and matching the inflow data,

$$\alpha - \beta\xi_k + E(0, \xi_k, \boldsymbol{\nu}) = \psi_j^n(\xi_k), \quad \alpha + \beta(\Delta x + \xi_k) + E(\Delta x, -\xi_k, \boldsymbol{\nu}) = \psi_{j+1}^n(-\xi_k).$$

Following [32, 33] and [31], the Godunov scheme for (35) reads:

$$\begin{cases} \psi_j^{n+1}(\xi_k) = \psi_j^n(\xi_k) - \xi_k \dfrac{\Delta t}{\Delta x} \left(\psi_j^n(\xi_k) - \tilde{\psi}_{R,j-\frac{1}{2}}(\xi_k) \right), \\ \psi_j^{n+1}(-\xi_k) = \psi_j^n(-\xi_k) + \xi_k \dfrac{\Delta t}{\Delta x} \left(\tilde{\psi}_{L,j+\frac{1}{2}}(-\xi_k) - \psi_j^n(-\xi_k) \right), \end{cases} \tag{38}$$

where the left/right states $\tilde{\psi}_{L,j+\frac{1}{2}}(-\boldsymbol{\xi})$ and $\tilde{\psi}_{R,j-\frac{1}{2}}(\boldsymbol{\xi})$ are deduced from the previous numerical approximation of the steady-state curves for (14), that is,

$$\tilde{\psi}_{L,j+\frac{1}{2}}(-\xi_k) = \alpha + \beta\xi_k + E(0, -\xi_k, \boldsymbol{\nu}),$$

and, with the set of coefficients α, β, $\mathbf{A}$ and $\mathbf{B}$ computed at $x_{j-\frac{1}{2}}$,

$$\tilde{\psi}_{R,j-\frac{1}{2}}(\xi_k) = \alpha + \beta(\Delta x - \xi_k) + E(\Delta x, \xi_k, \boldsymbol{\nu}).$$

Clearly, it is more efficient to compute each $\tilde{\psi}_{L/R,j+\frac{1}{2}}(\pm\boldsymbol{\xi})$ out of $\psi_{j/j+1}^n(\pm\boldsymbol{\xi})$ by means of matrix operations. However, the scheme (38) is not suitable for direct implementation because in order to compute the set of coefficients, one would have to invert a matrix containing both $\exp(\Delta x/\nu_\ell) > 1$ and $\exp(-\Delta x/\nu_\ell) < 1$ terms.

To fix this defect, we modify the expansion (37) by changing the $N-1$ coefficients

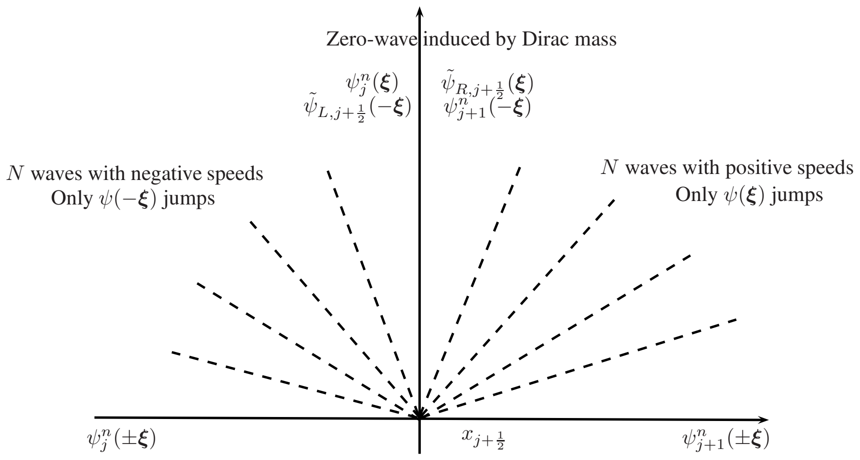

FIGURE 3. Self-similar solution of non-conservative Riemann problem.

$B_\ell \to B_\ell \exp(\Delta x/\nu_\ell)$ which leads to inverting the following linear problem:

$$M \begin{pmatrix} \boldsymbol{A} \\ \alpha \\ \boldsymbol{B} \\ \beta \end{pmatrix} = \begin{pmatrix} \psi_j^n(\boldsymbol{\xi}) \\ \psi_{j+1}^n(-\boldsymbol{\xi}) \end{pmatrix} \in \mathbb{R}^{2N},$$

where the $2N \times 2N$ matrix M reads for[5] $\boldsymbol{\nu} := \{\nu_1, \nu_2, ..., \nu_{N-1}\} \in (0, \xi_{max})^{N-1}$,

$$M = \begin{pmatrix} \left(1 - \boldsymbol{\xi} \otimes \boldsymbol{\nu}^{-1}\right)^{-1} & 1_{\mathbb{R}^N} & \left(1 + \boldsymbol{\xi} \otimes \boldsymbol{\nu}^{-1}\right)^{-1} \exp(-\frac{\Delta x}{\boldsymbol{\nu}}) & -\boldsymbol{\xi} \\ \left(1 + \boldsymbol{\xi} \otimes \boldsymbol{\nu}^{-1}\right)^{-1} \exp(-\frac{\Delta x}{\boldsymbol{\nu}}) & 1_{\mathbb{R}^N} & \left(1 - \boldsymbol{\xi} \otimes \boldsymbol{\nu}^{-1}\right)^{-1} & \Delta x + \boldsymbol{\xi} \end{pmatrix}.$$

By defining the complementary matrix,

$$\tilde M = \begin{pmatrix} \left(1 - \boldsymbol{\xi} \otimes \boldsymbol{\nu}^{-1}\right)^{-1} \exp(-\frac{\Delta x}{\boldsymbol{\nu}}) & 1_{\mathbb{R}^N} & \left(1 + \boldsymbol{\xi} \otimes \boldsymbol{\nu}^{-1}\right)^{-1} & \Delta x - \boldsymbol{\xi} \\ \left(1 + \boldsymbol{\xi} \otimes \boldsymbol{\nu}^{-1}\right)^{-1} & 1_{\mathbb{R}^N} & \left(1 - \boldsymbol{\xi} \otimes \boldsymbol{\nu}^{-1}\right)^{-1} \exp(-\frac{\Delta x}{\boldsymbol{\nu}}) & \boldsymbol{\xi} \end{pmatrix},$$

one observes that, for any $j \in \mathbb{Z}$, the interface values in (38) are given by:

$$\begin{pmatrix} \tilde\psi_{R,j+\frac12}(\boldsymbol{\xi}) \\ \tilde\psi_{L,j+\frac12}(-\boldsymbol{\xi}) \end{pmatrix} = \tilde M \; M^{-1} \begin{pmatrix} \psi_j^n(\boldsymbol{\xi}) \\ \psi_{j+1}^n(-\boldsymbol{\xi}) \end{pmatrix}. \tag{39}$$

Therefore, the correct way to implement the well-balanced Godunov scheme for (14) consists in iterating in time (38) after having previously computed all the necessary interface values using (39). Obviously, the product $\tilde M M^{-1}$ must be performed before setting up the time-marching process. Numerical results on the classical Couette flow obtained with this numerical algorithm will be displayed in §4.

[5]The value ν_N is meaningless for a conservative equation [6].

3.3. **Complete time-dependent scheme for heat transfer.** We now proceed to handle numerically the 2×2 system extracted from the two first lines of (12)–(13); for ease of writing, we shall hereafter use the notation Ψ for the vector of $\mathbb{R}^2$ which reads $\Psi(t,x,\xi) = (\Psi_1 \ \Psi_2)^T$. According to §2.1, this vector is solution of the initial/boundary value problem for:

$$\partial_t \Psi + \xi \partial_x \Psi = \left(\int_{\mathbb{R}} [\mathbf{P}(\xi)\mathbf{P}(\xi')^T + 2\xi\xi' \begin{pmatrix} 1 & 0 \\ 0 & 0 \end{pmatrix}] \Psi(x,\xi') \frac{\exp(-|\xi'|^2)}{\sqrt{\pi}} d\xi' \right) - \Psi,$$

where the matrix $\mathbf{P}$ reads,

$$\mathbf{P}(\xi) = \begin{pmatrix} \sqrt{\frac{2}{3}}(\xi^2 - \frac{1}{2}) & 1 \\ \sqrt{\frac{2}{3}} & 0 \end{pmatrix}.$$

The derivation of the well-balanced Godunov scheme for this problem follows the same canvas as [31] or the former subsection; in particular, the same computational grid (34) and the same Gaussian quadrature rule (29) will be used in order to produce a piecewise constant approximation of Ψ:

$$\forall j,n \in \mathbb{Z} \times \mathbb{N}, \qquad \Psi_j^n(\pm\boldsymbol{\xi}) \simeq \Psi(t^n, x_j, \pm\boldsymbol{\xi}) \in \mathbb{R}^2.$$

The first step is to localize the integral collision term on the discrete lattice $(j + \frac{1}{2})\Delta x$, $j \in \mathbb{Z}$ by means of Dirac masses, exactly like in (35). This process induces a countable sum of non-conservative products on the right-hand side of the localized equation; these singular products vanish for $x \neq x_{j+\frac{1}{2}}$. The structure of the resulting non-conservative Riemann problems is identical to the one displayed on Fig. 3. We thus proceed to explain how the stationary solutions satisfying the boundary value problem for (22) can be computed in practice at each interface $x = x_{j+\frac{1}{2}}$ following ideas originally proposed by Siewert in [60] (see again Appendix A). Since $|\mathbf{P}(\xi)| = -\sqrt{2/3} \neq 0$ for any value of $\xi \in \mathbb{R}$, one can define:

$$\Upsilon(x,\xi) = \mathbf{P}(\xi)^{-1}\Psi(x,\xi), \qquad \mathbf{S}(\xi) = \mathbf{P}(\xi)^T \mathbf{P}(\xi) \frac{\exp(-\xi^2)}{\sqrt{\pi}}.$$

The aforementioned 2×2 matrix $\mathbf{S}$ is clearly symmetric and moreover,

$$\forall \xi \in \mathbb{R}, \qquad \mathbf{S}(-\xi) = \mathbf{S}(\xi).$$

Hence, assuming the macroscopic flux term vanishes, it comes from (22) that:

$$\xi \partial_x \Upsilon + \Upsilon = \int_0^\infty [\Upsilon(x,\xi') + \Upsilon(x,-\xi')]\mathbf{S}(\xi') d\xi', \tag{40}$$

which is an expression quite similar to (30). By the classical separation of variables trick, one writes for some separation constant $\nu \neq 0$ and a function $\boldsymbol{\varphi} \in \mathbb{R}^2$:

$$\forall k \in \{1,2,...,N\}, \qquad \Upsilon(x, \pm\xi_k) = \boldsymbol{\varphi}(\nu, \pm\xi_k) \exp(-x/\nu).$$

Approximating the semi-infinite integrals in (40) by finite sums yields:

$$\left(1 \mp \frac{\xi_k}{\nu}\right) \boldsymbol{\varphi}(\nu, \pm\xi_k) = \sum_{\ell=1}^N \omega_\ell [\boldsymbol{\varphi}(\nu, \xi_\ell) + \boldsymbol{\varphi}(\nu, -\xi_\ell)] \mathbf{S}(\xi_\ell).$$

At this point, and for any value of ν, the following 2 vectors can be defined:

$$\boldsymbol{\varphi}_{i,\pm}(\nu,\boldsymbol{\xi}) = \begin{pmatrix} \boldsymbol{\varphi}_i(\nu,\pm\xi_1) \\ \boldsymbol{\varphi}_i(\nu,\pm\xi_2) \\ \dots \\ \boldsymbol{\varphi}_i(\nu,\pm\xi_N) \end{pmatrix} \in \mathbb{R}^N, \qquad i \in \{1,2\}.$$

And, for $\boldsymbol{\varphi}_\pm := (\boldsymbol{\varphi}_{1,\pm}^T\ \boldsymbol{\varphi}_{2,\pm}^T)^T \in \mathbb{R}^{2N}$, the $2N \times 2N$ weight matrix

$$W := \begin{pmatrix} W_{1,1} & W_{1,2} \\ W_{2,1} & W_{2,2} \end{pmatrix}, \qquad (W_{m,n})_{k,\ell} = \omega_\ell \mathbf{S}_{m,n}(\xi_\ell),$$

and the $2N \times 2N$ invertible diagonal matrix $D = diag(\boldsymbol{\xi}\ \boldsymbol{\xi})$, it comes that:

$$D^{-1}(Id - 2W)D^{-1}[D(\boldsymbol{\varphi}_+ + \boldsymbol{\varphi}_-)] = \frac{1}{\nu^2}[D(\boldsymbol{\varphi}_+ + \boldsymbol{\varphi}_-)].$$

This eigenvalue problem for $\boldsymbol{\nu}$ only produces a set of $2N$ approximate constants of separation, among which 2 are meaningless as they correspond to collisional invariants. One can observe that this procedure is more efficient when it comes to practical implementation compared to the solving of (26). According to the general expression of the solution (23), a convenient numerical approximation of the stationary equation posed in the interval $x \in (0,\Delta x)$ reads:

$$\Psi(x,\pm\xi_k) = \sum_{i=1}^{2} \mathbf{P}(\pm\xi_k)[\alpha_i + \beta_i(x \mp \xi_k)]\vec{e}_i + \mathbf{P}(\pm\xi_k)\mathbf{E}(x,\pm\xi_k,\boldsymbol{\nu}). \tag{41}$$

where, analogously with the scalar formula (37), $\mathbf{E}$ stands for the finite superimposition of exponentially damped modes,

$$\mathbf{E}(x,\pm\xi,\boldsymbol{\nu}) = \sum_{\ell=1}^{2N-2} \left(\frac{A_\ell}{1-\xi/\nu_\ell}\exp(-x/\nu_\ell) + \frac{B_\ell}{1+\xi/\nu_\ell}\exp(x/\nu_\ell) \right) \tilde{\mathbf{R}}(\nu_\ell), \tag{42}$$

and finally, the vectors $\tilde{\mathbf{R}}(\nu_\ell)$ are numerical approximations of the exact ones computed in (25). Each one belongs to the null-space of the following 2×2 matrix:

$$\Omega(\nu_\ell) = Id - 2\sum_{k=1}^{N} \left(\frac{\omega_k}{1-(\nu_\ell/\xi_k)^2}\mathbf{S}(\xi_k) \right), \qquad \Omega(\nu_\ell)\tilde{\mathbf{R}}(\nu_\ell) = \vec{0},$$

for any index $\ell \in \{1,2,...,2N-2\}$. The factor 2 results from the fact that $\mathbf{S}$ and ξ^2 are even functions, which allows to reduce (25) to the approximation of a semi-infinite integral by means of the Gaussian quadrature rule (29). Clearly, from the knowledge of the inflow boundary conditions at each extremity of the computational domain, it is possible to compute the approximation (41) at any location $x, \xi_k \in (0,\Delta x)\times\boldsymbol{\xi}$ by inverting a matrix for the set of coefficients $\alpha_{1,2}, \beta_{1,2}, A_\ell, B_\ell$. However, as it has been noticed in §3.2, such a matrix would contain both $\exp(\Delta x/\nu_\ell) > 1$ and $\exp(-\Delta x/\nu_\ell) < 1$ terms, which may generate some instability. It is therefore convenient to rescale again the coefficients $B_\ell \to B_\ell \exp(\Delta x/\nu_\ell)$ in order to solve a linear system of equations involving the $4N \times 4N$ following matrix:

$$M = \begin{pmatrix} \frac{\mathbf{P}(\boldsymbol{\xi})\otimes\tilde{\mathbf{R}}(\boldsymbol{\nu})}{1-(d\boldsymbol{\xi})\otimes\boldsymbol{\nu}^{-1}} & \mathbf{P}(\boldsymbol{\xi})[\vec{e}_1\ \vec{e}_2] & \frac{\mathbf{P}(\boldsymbol{\xi})\otimes\tilde{\mathbf{R}}(\boldsymbol{\nu})}{1+(d\boldsymbol{\xi})\otimes\boldsymbol{\nu}^{-1}}\exp\left(-\frac{\Delta x}{\boldsymbol{\nu}}\right) & -\mathbf{P}(\boldsymbol{\xi})d\boldsymbol{\xi}[\vec{e}_1\ \vec{e}_2] \\ \frac{\mathbf{P}(\boldsymbol{\xi})\otimes\tilde{\mathbf{R}}(\boldsymbol{\nu})}{1+(d\boldsymbol{\xi})\otimes\boldsymbol{\nu}^{-1}}\exp\left(-\frac{\Delta x}{\boldsymbol{\nu}}\right) & \mathbf{P}(\boldsymbol{\xi})[\vec{e}_1\ \vec{e}_2] & \frac{\mathbf{P}(\boldsymbol{\xi})\otimes\tilde{\mathbf{R}}(\boldsymbol{\nu})}{1-(d\boldsymbol{\xi})\otimes\boldsymbol{\nu}^{-1}} & \mathbf{P}(\boldsymbol{\xi})(\Delta x + d\boldsymbol{\xi})[\vec{e}_1\ \vec{e}_2] \end{pmatrix}$$

where the fraction bar means here component-wise division,

$$\boldsymbol{\nu} := \{\nu_1, \nu_2, ..., \nu_{2N-2}\} \in \mathbb{R}^{2N-2},$$

and d stands for the $2N \times N$ "doubling matrix",

$$d = \begin{pmatrix} 1 & 0 & 0 & \dots & 0 \\ 1 & 0 & 0 & \dots & 0 \\ 0 & 1 & 0 & \dots & 0 \\ 0 & 1 & 0 & \dots & 0 \\ \vdots & & & & \vdots \\ 0 & 0 & \dots & 0 & 1 \\ 0 & 0 & \dots & 0 & 1 \end{pmatrix}, \qquad d\boldsymbol{\xi} = \begin{pmatrix} \xi_1 \\ \xi_1 \\ \xi_2 \\ \xi_2 \\ \vdots \\ \xi_N \\ \xi_N \end{pmatrix} \in \mathbb{R}^{2N}.$$

At each interface $x_{j+\frac{1}{2}}$ between the computational cells C_j and C_{j+1}, the set of $4N$ coefficients $\alpha_{1,2}, \beta_{1,2}, A_\ell, B_\ell$ satisfying the compatibility conditions is sought:

$$\Psi(0, \xi_k) = \Psi_j^n(\xi_k), \qquad \Psi(\Delta x, -\xi_k) = \Psi_{j+1}^n(-\xi_k). \tag{43}$$

Thanks to the preceding definition of M, the resolution of the equations (41)-(42) is reduced to the inversion of the linear system:

$$M \begin{pmatrix} \boldsymbol{A} \in \mathbb{R}^{2N-2} \\ \alpha_1 \\ \alpha_2 \\ \boldsymbol{B} \in \mathbb{R}^{2N-2} \\ \beta_1 \\ \beta_2 \end{pmatrix} = \begin{pmatrix} \Psi_j^n(\boldsymbol{\xi}) \in \mathbb{R}^{2N} \\ \Psi_{j+1}^n(-\boldsymbol{\xi}) \in \mathbb{R}^{2N} \end{pmatrix}.$$

From (43), one computes easily:

$$\tilde{\Psi}_{R,j+\frac{1}{2}}(\xi_k) = \Psi(\Delta x, \xi_k), \qquad \tilde{\Psi}_{L,j+\frac{1}{2}}(-\xi_k) = \Psi(0, -\xi_k), \tag{44}$$

and those are precisely the values which are necessary in order to set up a well-balanced Godunov scheme for the 2×2 system extracted from (12)–(13):

$$\begin{cases} \Psi_j^{n+1}(\xi_k) = \Psi_j^n(\xi_k) - \xi_k \dfrac{\Delta t}{\Delta x}\left(\Psi_j^n(\xi_k) - \tilde{\Psi}_{R,j-\frac{1}{2}}(\xi_k)\right), \\ \Psi_j^{n+1}(-\xi_k) = \Psi_j^n(-\xi_k) + \xi_k \dfrac{\Delta t}{\Delta x}\left(\tilde{\Psi}_{L,j+\frac{1}{2}}(-\xi_k) - \Psi_j^n(-\xi_k)\right). \end{cases} \tag{45}$$

As for the treatment of the reduced viscosity equation, the computation of the set of aforementioned coefficients is not necessary: it suffices to introduce another matrix $\tilde{M}$ which reads, (with the same notations as the ones used in M)

$$\tilde{M} = \begin{pmatrix} \frac{\mathbf{P}(\boldsymbol{\xi}) \otimes \tilde{\mathbf{R}}(\boldsymbol{\nu})}{1-(d\boldsymbol{\xi}) \otimes \boldsymbol{\nu}^{-1}} \exp\left(-\frac{\Delta x}{\boldsymbol{\nu}}\right) & \mathbf{P}(\boldsymbol{\xi})[\vec{e}_1 \ \vec{e}_2] & \frac{\mathbf{P}(\boldsymbol{\xi}) \otimes \tilde{\mathbf{R}}(\boldsymbol{\nu})}{1+(d\boldsymbol{\xi}) \otimes \boldsymbol{\nu}^{-1}} & \mathbf{P}(\boldsymbol{\xi})(\Delta x - d\boldsymbol{\xi})[\vec{e}_1 \ \vec{e}_2] \\ \frac{\mathbf{P}(\boldsymbol{\xi}) \otimes \tilde{\mathbf{R}}(\boldsymbol{\nu})}{1+(d\boldsymbol{\xi}) \otimes \boldsymbol{\nu}^{-1}} & \mathbf{P}(\boldsymbol{\xi})[\vec{e}_1 \ \vec{e}_2] & \frac{\mathbf{P}(\boldsymbol{\xi}) \otimes \tilde{\mathbf{R}}(\boldsymbol{\nu})}{1-(d\boldsymbol{\xi}) \otimes \boldsymbol{\nu}^{-1}} \exp\left(-\frac{\Delta x}{\boldsymbol{\nu}}\right) & \mathbf{P}(\boldsymbol{\xi}) d\boldsymbol{\xi}[\vec{e}_1 \ \vec{e}_2] \end{pmatrix},$$

in order to derive the relation at each interface in the computational domain:

$$\begin{pmatrix} \tilde{\Psi}_{R,j+\frac{1}{2}}(\boldsymbol{\xi}) \\ \tilde{\Psi}_{L,j+\frac{1}{2}}(-\boldsymbol{\xi}) \end{pmatrix} = \tilde{M} \ M^{-1} \begin{pmatrix} \Psi_j^n(\boldsymbol{\xi}) \\ \Psi_{j+1}^n(-\boldsymbol{\xi}) \end{pmatrix}. \tag{46}$$

Obviously, the matrix inversion/product $\tilde{M}.M^{-1}$ has to be performed before starting the iterations in time. This derivation of interface values offers 2 advantages:

1. The scheme (45)–(46) is completely linear thus there's no substantial obstacle for making it implicit in time in order to go beyond the usual CFL restriction.

$N = 10$	1.171642
$N = 15$	1.241705
$N = 25$	1.395569
$N = 40$	1.663094

TABLE 1. Condition numbers for the product $\tilde{M}\ M^{-1}$.

2. The condition number of the matrix product $\tilde{M}\ M^{-1}$ remains very close to unity for several values of N between 10 and 40 which is a good sign for general stability (see Table 1 with $\Delta x = 2^{-5}$).

Therefore, the set of relations (45) and (46) constitutes the correct way to implement the well-balanced Godunov scheme on the subsystem of (12) describing density fluctuations and heat transfer effects. Its practical realizability and its accuracy will be checked in the forthcoming §5 and §6.

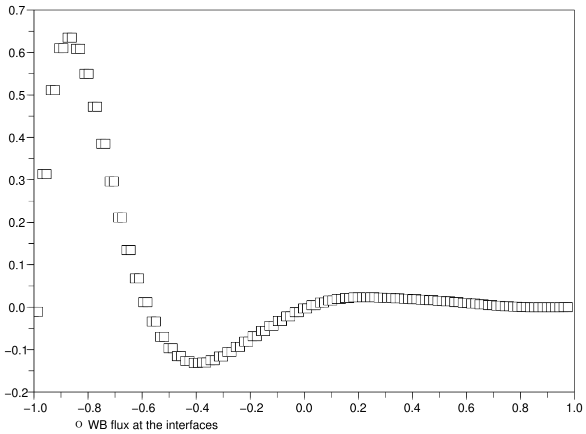

FIGURE 4. Macroscopic fluxes computed on both sides L/R of each computational cell's interface in transitory regime.

Remark 3. In order to be able to generate a stationary numerical solution endowed with a constant macroscopic flux, it is necessary to check that the scheme (45) uses values at the interface of each computational cells $\Psi_{L/R,j+\frac{1}{2}}(\boldsymbol{\xi})$ for which the flux conservation holds: for any $j, n \in \mathbb{Z} \times \mathbb{N}$,

$$\vec{e}_1 . \sum_{k=1}^{N} \omega_k \xi_k \Big([\Psi_j^n(\xi_k) - \Psi_{L,j+\frac{1}{2}}(-\xi_k)] - [\Psi_{R,j+\frac{1}{2}}(\xi_k) - \Psi_{j+1}^n(-\xi_k)] \Big) \exp(-\xi_k^2) = 0.$$

This is actually what happens as one can check on Fig.4 where we display the values of the macroscopic flux on each side of all the interfaces of the computational domain during some transient computation. Another important quantity is the heat flow, which, as a function of Ψ, reads

$$q(t,x) = \int_{\mathbb{R}} \xi \begin{pmatrix} \xi^2 - \frac{3}{2} \\ 1 \end{pmatrix} . \Psi(t,x,\xi) \frac{\exp(-\xi^2)}{\sqrt{\pi}} d\xi, \tag{47}$$

and is approximated by

$$q(t^n, x_j) \simeq \sum_{k=1}^{N} \omega_k \xi_k \begin{pmatrix} \xi_k^2 - \frac{3}{2} \\ 1 \end{pmatrix} .[\Psi_j^n(\xi_k) - \Psi_j^n(-\xi_k)] \frac{\exp(-\xi_k^2)}{\sqrt{\pi}}.$$

When the well-balanced scheme reaches steady-state, both the macroscopic mass and heat fluxes stabilize onto a constant[6] up to small errors related to the Gaussian quadrature (29): see practical illustrations on Figs. 11 and 13.

3.4. **A link with Liu-Yang-Yu's "micro-macro decomposition".** When choosing this different approach, one starts by considering the Boltzmann equation (1) with its right-hand side divided by a small number ε (related to the molecules mean free path) inside which the following decomposition is plugged:

$$f(t, \mathbf{x}, \mathbf{v}) = M(t, \mathbf{x}, \mathbf{v}) + \varepsilon g.$$

The quantity $M(t, \mathbf{x}, \mathbf{v})$ is the local Maxwellian distribution completely determined by the 5 first moments of f in the $\mathbf{v}$ variable. By exploiting the bilinearity of Q and the property $Q(M, M) = 0$, (1) is reduced to:

$$\partial_t M + \mathbf{v}.\nabla_{\mathbf{x}} M + \varepsilon(\partial_t g + \mathbf{v}.\nabla_{\mathbf{x}} g) = L_M g + \varepsilon Q(g, g). \tag{48}$$

Next, one observes that for each $t, \mathbf{x}$, the linearized operator L_M admits a null space which is spanned by the orthogonal basis $M(t, \mathbf{x}, \mathbf{v})\Phi(\mathbf{v})$. Thus an analogue of the orthogonal projector $\mathcal{P}$, denoted Π_M in [13], is introduced. The algorithm proceeds by letting Π_M act on (48): for instance, Proposition 3.2 in [13] states precisely what coupled system one gets by means of this method for the BGK model (4) of the Boltzmann equation with $\nu = \frac{1}{\varepsilon}$ when $\mathbf{v} \in \mathbb{R}$ is one-dimensional. Several relations exist between this approach and the present well-balanced strategy:

1. The separation fluid/microscopic variables is automatic in (19) and (23): in particular, there is no need to decompose the initial data.
2. The implementation of boundary conditions is straightforward for the well-balanced schemes (38) and (45) because both act directly on kinetic variables (the decomposition fluid/microscopic is carried out inside the numerical fluxes at each cell's interfaces through (39) and (46)): in particular, implementing walls with accommodation coefficients different from 0 or 1 may be delicate in the schemes presented in [30, 13].
3. There is in general no well-balanced property built in the micro-macro algorithms: one may be tempted to wonder how quantities supposedly constant at steady-state are rendered with these schemes for $\varepsilon \simeq 1$.
4. The micro-macro algorithms are able to handle non-linear collision terms, and this is not yet doable in the present well-balanced methodology. Indeed, when the stationary equations become non-linear, the superposition principle leading to the elementary solutions decomposition cannot hold true.

4. Numerical results for transient Couette flow.

4.1. **Implementation of boundary conditions.** In this subsection, we mainly follow [70] (see also [9, 10, 6, 57]) in order to demonstrate the high accuracy achieved by the well-balanced Godunov scheme (38)–(39) when solving (14) in the context of the classical Couette flow for a viscous incompressible fluid. In particular, the behavior of shear stress at steady-state will be displayed.

[6]If the macroscopic mass flux vanishes, the walls are said to have "thermalized" the gas [27].

Remark 4. Let us note at once that in [70, 6], the authors considered moments of the kinetic density h simply against $\mathbf{v}_{2\ or\ 3}\exp(-\mathbf{v}_2^2-\mathbf{v}_3^2)/\pi$ whereas the functions written in (9) are orthonormal. There is thus a $\sqrt{\frac{\pi}{2}}$ normalization factor between both models (see *e.g.* formulas (48)–(49) in [70]).

The implementation of boundary conditions is done according to what Cercignani [23] calls the simplest kernel model (on page 73) which reads in one dimension,

$$R(\xi' \to \xi) = \alpha F(\xi) + (1-\alpha)\delta(\xi+\xi'),$$

where the parameter $\alpha \in [0,1]$ is called the "accommodation coefficient" and accounts for the proportion of molecules which undergo a specular reflexion while the remaining fraction is dragged by the transverse movement of the walls. When $\alpha = 1$, one speaks about no-slip boundary conditions because the fluid has zero velocity relative to the boundary. In our context, this means that all the molecules hitting the walls get stuck at these boundaries and thus are completely driven by their transverse movement. For any value of $\alpha \in [0,1]$, it is well-known that the (1,3)-component in the pressure tensor (one may also speak about the normalized shear stress, see formula (15) in [6]) must be a constant at steady-state. Indeed, this quantity reads:

$$p_{1,3}(t,x) = \frac{1}{\sqrt{2\pi}} \int_{\mathbb{R}} \xi\psi(t,x,\xi)\frac{\exp(-\xi^2)}{\sqrt{\pi}}d\xi, \tag{49}$$

and its x-derivative must vanish at the steady-state of (14). In general, time-splitting schemes aren't endowed with this type of property, even in a somewhat simpler context of quasilinear hyperbolic systems of conservation laws with source terms, and we shall see that the discrepancy can be important for Couette flow.

4.2. **No-slip condition:** $\alpha = 1$**.** In this case, the gas velocity at each fluid/solid boundary equals the one of solid boundary: according to [70], the kinetic density h must be proportional to the one of the wall, denoted by $u_{wall} > 0$,

$$h\left(t, \mathbf{x} = \{\pm 1\} \times \mathbb{R}^2, \mathbf{v} \in \mathbb{R}^{\mp} \times \mathbb{R}^2\right) = \lambda u_{wall}\mathbf{v}_3. \tag{50}$$

Thus, applying the definition given by the orthonormal functions (9), one obtains:

$$\psi(t, x = \pm 1, \mp|\xi|) = \lambda u_{wall}\sqrt{\frac{2}{\pi}} \underbrace{\int_{\mathbb{R}^2} \mathbf{v}_3^2 \exp(-\mathbf{v}_2^2 - \mathbf{v}_3^2)d\mathbf{v}_2 d\mathbf{v}_3}_{=\sqrt{\pi}\times\sqrt{\pi}/2=\pi/2} = \lambda u_{wall}\sqrt{\frac{\pi}{2}}.$$

Hence in order to ensure that $\psi(t, x = \pm 1, \mp|\xi|) = \mp u_{wall}$ can hold, it is necessary to fix $\lambda = \sqrt{\frac{2}{\pi}}$. In [70, 6], the authors used a different normalization constant, $\frac{1}{\pi}$ instead of $\sqrt{\frac{2}{\pi}}$, thus they are led to select $\lambda = 2$. On Fig.5, we display the steady-state obtained by iterating in time the well-balanced scheme (38)–(39) for $u_{wall} = 1$ until convergence of the residues up to 10^{-15}; this happens for $t \simeq 100$ with a CFL number of 0.9, a value of $\xi_{max} = 3.5$, $N = 25$ (that is, 50 grid points in the velocity variable) and 2^6 points griding the computational domain $x \in (-1,1)$. The quantities shown on this figure are respectively the transverse momentum (20) (top, left), the shear stress (49) (top, right), the kinetic density ψ visualized in the plane x, ξ (bottom, right) and the residues decay in logarithmic scale (bottom, left). The initial data has been chosen very far away from the equilibrium distribution like in the numerical tests studied in [31]: anyway, we observe a monotonic decay and a global stabilization of the numerical process. In particular, the normalized

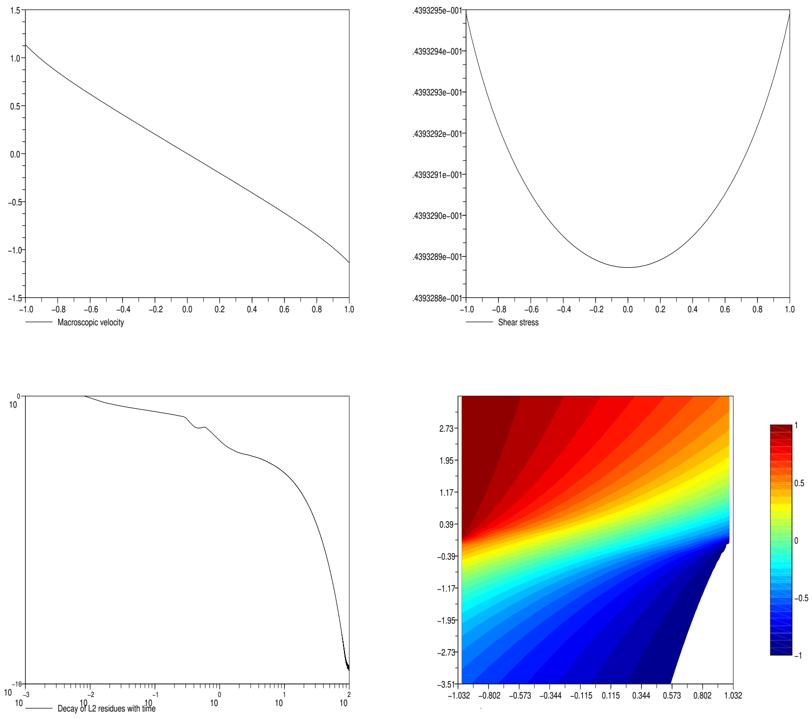

FIGURE 5. Results of (38)–(39) for $\alpha = 1$ at time $t = 100$.

stress at numerical steady-state varies between 0.4393288 and 0.4393294, thus it can be considered as a constant in practice. At this point, we wanted to investigate

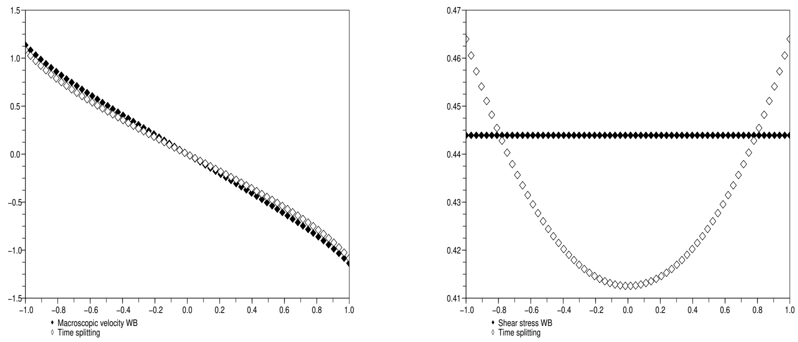

FIGURE 6. Comparison between well-balanced and time-splitting schemes for (14): transverse momentum (left), shear stress (right).

whether or not a more classical time-splitting discretization was able to reach a steady-state with similar properties [27, 28]. Thus a straightforward time-splitting marching scheme has been set up for solving the reduced viscosity equation (14):

the outcome of both numerical processes is shown on Fig. 6. Needless to say, the unphysical character of the shear stress generated by the time-splitting scheme is very apparent as it displays a relative variation of the order of 12.7%. The one computed by the well-balanced scheme (38)–(39) appears constant in comparison. We checked that this constant value is very close to the ones given by Cercignani in his book [23] on page 121: for a Knudsen number of 2, values of the shear stress between 0.4437 and 0.444 are obtained with 3 different methods. This is compatible with the results generated by the scheme (38)–(39). Concerning the little overshoot of the macroscopic momentum over 1, we believe that this comes from the Gaussian quadrature and the relatively small value of ξ_{max} because both the well-balanced and the time-splitting schemes display this feature. It is therefore not related to the way the integral collision term gets treated numerically.

4.3. **Partial specular reflexion:** $\alpha = \frac{1}{2}$. Now we have in mind to compute a more complex situation, where molecules can undergo both the dragging effect of the transverse movement of the walls and specular reflexion. Therefore, (50) has to be substituted with a more general expression holding for any $\alpha \in [0, 1]$:

$$h\left(t, \mathbf{x} = \{\pm 1\} \times \mathbb{R}^2, \mathbf{v}_1 \in \mathbb{R}^{\mp}, \mathbf{v}_2, \mathbf{v}_3\right) = \alpha \sqrt{\frac{2}{\pi}} u_{wall} \mathbf{v}_3 + (1-\alpha) h\left(t, \mathbf{x}, -\mathbf{v}_1, \mathbf{v}_2, \mathbf{v}_3\right).$$

Taking again moments according to (9), we obtain the boundary conditions for ψ:

$$\psi(t, x = \pm 1, \mp|\xi|) = \mp \alpha u_{wall} + (1-\alpha)\psi(t, x = \pm 1, \pm|\xi|).$$

On Fig. 7, we display the results obtained with the same parameters than the ones used in the preceding subsection, but with the notable difference coming from the accommodation coefficient $\alpha = \frac{1}{2}$. Clearly, the kinetic density at numerical steady-state (bottom, right) displayed in the x, ξ plane appears quite different compared to the one on Fig. 5. However, the shear stress (49) (top, right) keeps on being practically a constant: it varies between 0.3226598 and 0.3226603. It took roughly the same amount of time to get the residues to a value of the order of 10^{-9}, thus revealing a more delicate stabilization process. On Fig. 8, we show the comparison between the outcome of a classical time-splitting scheme for (14) with the accommodation coefficient $\alpha = \frac{1}{2}$ on each wall and the well-balanced scheme (38)–(39). The conclusions are similar to those in the preceding subsection: the time-splitting scheme seems to be unable to produce a constant shear stress at numerical steady-state whereas the well-balanced approach does. Interestingly, one can notice that the correct (constant) value computed by the well-balanced scheme is **not** close to the arithmetic average of the time-splitting approximation.

5. Numerical results for heat transfer and sound wave.

5.1. **Two “density bumps” with specular reflexion.** This subsection is devoted to illustrate the time evolution of the well-balanced Godunov scheme (45)–(46) when one applies an initial data of the same type as the ones used in [31]:

$$\Psi_1(t = 0, x, \xi) = \exp\left(-10(x \pm \frac{1}{2})^2 - 5(\xi \mp \frac{\xi_{max}}{2})^2\right), \qquad \xi \in \mathbb{R},$$

and the second component $\Psi_2(t = 0, x, \xi) = -0.75\Psi_1(t = 0, x, \xi)$. The simulation takes place in the computational domain $x \in (-1, 1)$ with purely specular boundary conditions at each border:

$$\forall t > 0, \qquad \Psi(t, x = \pm 1, \mp|\xi|) = \Psi(t, x = \pm 1, \pm|\xi|). \tag{51}$$

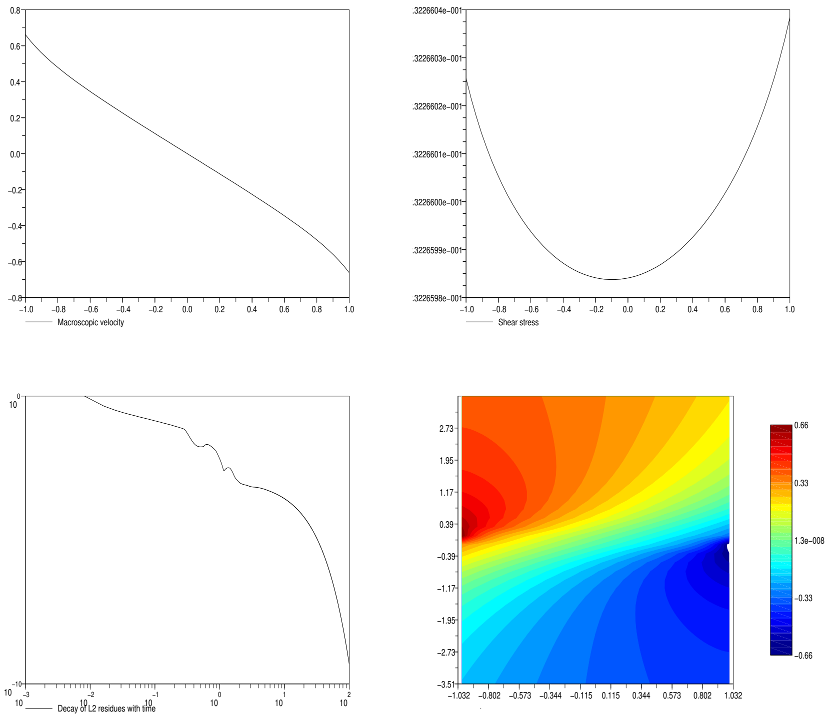

FIGURE 7. Well-balanced results with $\alpha = \frac{1}{2}$ at time $t = 100$.

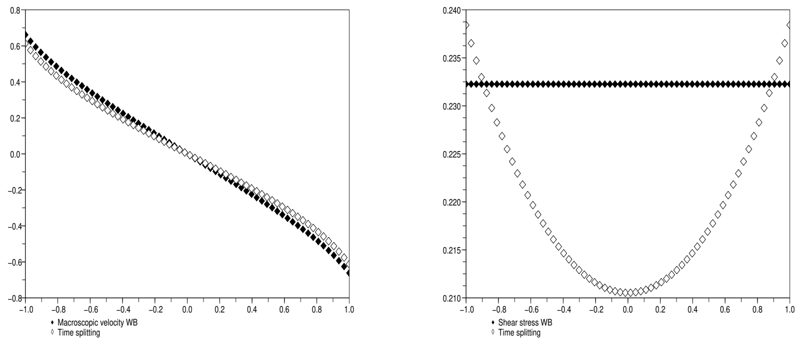

FIGURE 8. Comparison between well-balanced and time-splitting schemes for (14): transverse momentum (left), shear stress (right).

The parameters are identical to the ones used for the reduced viscosity equation in the preceding section. Numerical results for the first component of the transient kinetic density $\Psi_1(t, x, \xi) \exp(-\xi^2)$ in the x, ξ plane for $t = 0.15, 0.45, 1.55, 2.85$ are displayed on Fig.9. The mixing effect (entropy dissipation) of the integral collision term appears nicely and the symmetric character of the initial data survives as time

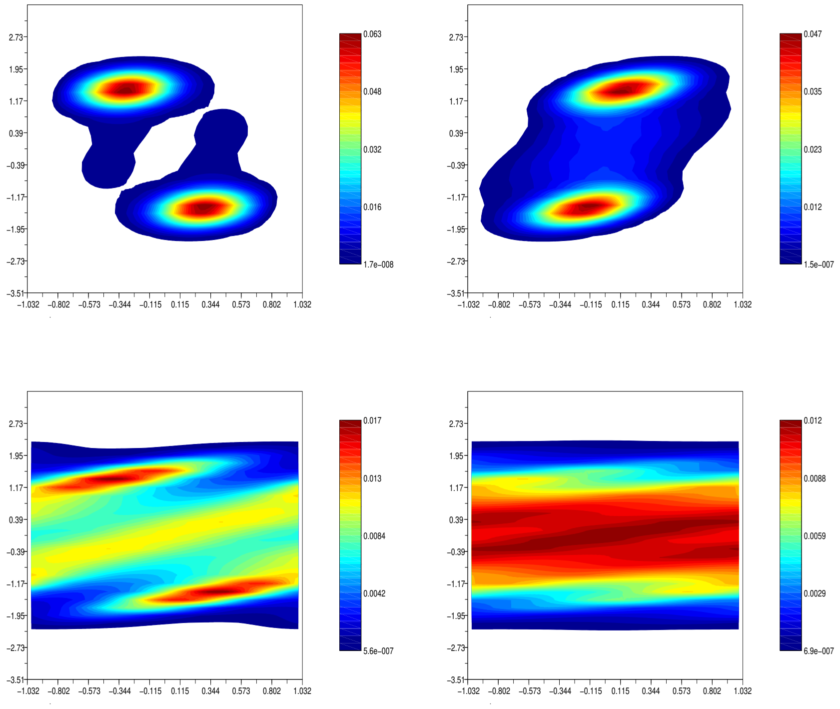

FIGURE 9. Kinetic density $\Psi_1(t,x,\xi)\exp(-\xi^2)$ at $t = 0.15, 0.45, 1.55, 2.85$.

increases. Neither spurious extrema nor oscillations show up despite the specular reflections (51) on the left and right borders are not likely to dampen them. According to both the quadrature rule (29) and the Remark 2, the numerical approximation of the macroscopic density and flux would read in the present context:

$$\left\{\begin{aligned} \varrho_j^n &= \left(\sum_{k=1}^{N} \omega_k \left(\Psi_j^n(\xi_k) + \Psi_j^n(-\xi_k)\right)\exp(-\xi_k^2)\right).\vec{e}_1 \simeq \varrho(t^n, x_j), \\ (\varrho\mathbf{u}_1)_j^n &= \left(\sum_{k=1}^{N} \omega_k \xi_k \left(\Psi_j^n(\xi_k) - \Psi_j^n(-\xi_k)\right)\exp(-\xi_k^2)\right).\vec{e}_1 \simeq \varrho\mathbf{u}_1(t^n, x_j). \end{aligned}\right. \tag{52}$$

5.2. **Walls with different temperatures:** $\alpha_1 = \alpha_2 = 1$**.** Hereafter we are concerned with heat transfer problems [9]: namely, we shall study the time evolution of Ψ when the walls located in $x = \pm 1$ are heated and thus locally increase the gas temperature. First, the case where both walls have opposite temperatures and the same accommodation coefficient, and second, when accommodation coefficients are different. Following [60, 70], we give the boundary conditions:

$$\forall t > 0, \qquad \Psi(t, \pm 1, \mp|\xi|) = (1-\alpha_i)\Psi(t, \pm 1, \pm|\xi|) \mp \alpha_i \delta_i \sqrt{\pi} \begin{pmatrix} \xi^2 + \beta_i \\ 1 \end{pmatrix}. \tag{53}$$

The coefficients $\alpha_i \in [0,1]$, $i = \{1,2\}$, are the accommodation coefficients of each wall, the ones denoted by $\delta_i = (T_i - T_0)/T_0$ stand for the deviation of the temperature of each wall with respect to a temperature of reference T_0 (which can be taken as $T_0 = \frac{1}{2}(T_1 + T_2)$). The coefficients β_i must be computed in order to ensure that the mass flux at the walls is always zero,

$$\forall t > 0, \qquad \vec{e}_1 . \int_{\mathbb{R}} \xi \Psi(t, x = \pm 1, \xi) \exp(-\xi^2) d\xi = 0.$$

We give some details about the computation of β_1 which is related to $x = -1$:

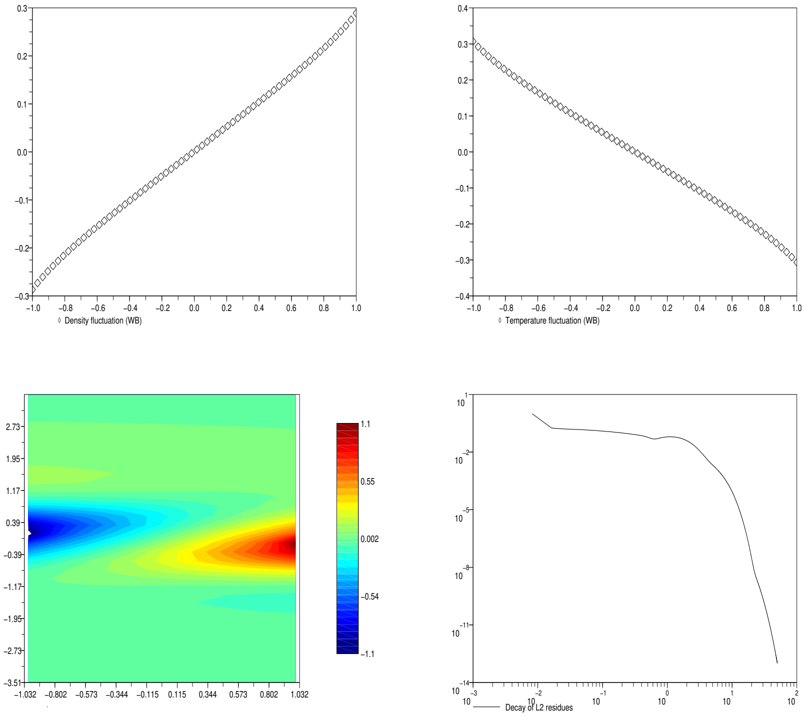

FIGURE 10. Macroscopic density and temperature fluctuation (top) at steady-state for $\delta_1 = -\delta_2 = \frac{1}{2}$, $\alpha_1 = \alpha_2 = 1$ at $t = 50$.

$$0 = \underbrace{\int_{-\infty}^{0} \xi \Psi_1(t, -1, \xi) \exp(-\xi^2) d\xi + (1 - \alpha_1) \int_0^\infty \xi \Psi_1(t, -1, -\xi) \exp(-\xi^2) d\xi}_{-\alpha_1 \int_0^\infty \xi \Psi(t,-1,-\xi).\vec{e}_1 \exp(-\xi^2) d\xi} + \alpha_1 \sqrt{\pi} \delta_1 \int_0^\infty (\xi^3 + \xi \beta_1) \exp(-\xi^2) d\xi.$$

Assuming that $\alpha_1 \neq 0$, one can simplify the preceding expression:

$$\int_0^\infty \xi \Psi(t, -1, -\xi).\vec{e}_1 \exp(-\xi^2) d\xi = \sqrt{\pi} \delta_1 \int_0^\infty (\xi^3 + \xi \beta_1) \exp(-\xi^2) d\xi$$

Thus it is possible to express β_1 as a function of the known quantities:

$$\beta_1 = \frac{\int_0^\infty \xi \left(\Psi(t, -1, -\xi).\vec{e}_1 - \sqrt{\pi} \delta_1 \xi^2 \right) \exp(-\xi^2) d\xi}{\sqrt{\pi} \delta_1 \int_0^\infty \xi \exp(-\xi^2) d\xi}. \tag{54}$$

The Gaussian integrals in (54) can be computed explicitly because

$$\int_0^\infty \xi \exp(-\xi^2) d\xi = \int_0^\infty \xi^3 \exp(-\xi^2) d\xi = \frac{1}{2},$$

hence the exact value of β_1 reads, (as done by Siewert in [60])

$$\beta_1 = -1 + 2\vec{e}_1 . \int_0^\infty \xi \Psi(t, -1, -\xi) \frac{\exp(-\xi^2)}{\sqrt{\pi}} d\xi.$$

However, we believe that one should better compute β_1 approximately according to the Gaussian quadrature (29) at each time step in order to ensure that the **numerical** macroscopic fluxes (52) actually vanish on each border of the computational domain. Clearly, the computation of β_2 for the wall located in $x = 1$ is completely similar thus we omit it. On Fig.10, numerical results at steady-state are shown for

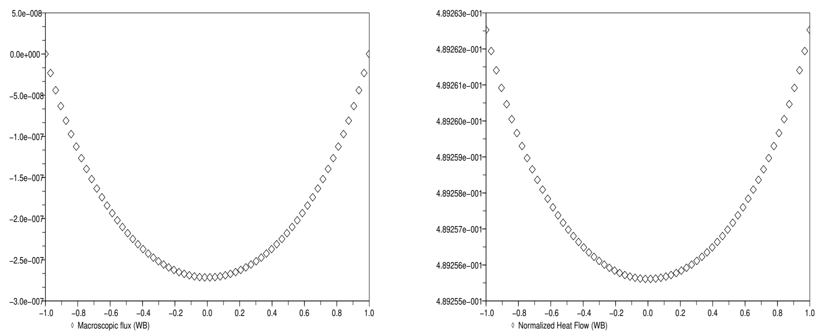

FIGURE 11. Constant quantities: mass flow (left) and heat flow (right).

$\delta_1 = -\delta_2 = \frac{1}{2}$ (meaning the wall in $x = -1$ is hot and the one in $x = 1$ is cold) and the same accommodation coefficient for each wall. The remaining computational parameters are the same than the ones chosen in the preceding sections. The kinetic density displayed in the x, ξ plane (bottom, left) is $\Psi \exp(-\xi^2).\vec{e}_1$, which first moment in ξ yields the macroscopic density ϱ (top, left). Logically, we find that the density is lower in the vicinity of the hot wall and bigger close to the cold one. The temperature decreases monotonically with x despite the specular reflexion taking place on each wall. At numerical steady-state, it is of critical importance to get constant mass and heat flows (47): actually, one can check on Fig.11 that despite the complexity of the test-case, they vary between 0 and 2.5×10^{-7}, 0.489255 and 0.489262, respectively. Such small variations allow to consider them as constant.

5.3. **Walls with different accommodation coefficients:** $\alpha_1 \neq \alpha_2$**.** Here, we consider a case similar to the preceding one, except that the walls have different accommodation coefficients; this has been already studied in *e.g.* [10] (see also [46, 47]) with different methods. Actually, the computation leading from (53) to (54) in the preceding subsection extends without difficulty to the case where $\alpha_1 \neq \alpha_2$. On Fig.12, we display numerical results at steady-state for the test-case considered in [60], which consists in fixing $\alpha_1 = 0.7$ and $\alpha_2 = 0.3$ with all the other parameters being kept equal. The first thing one can notice is that this seemingly little change implies that it takes twice the time to reach the numerical equilibrium. The

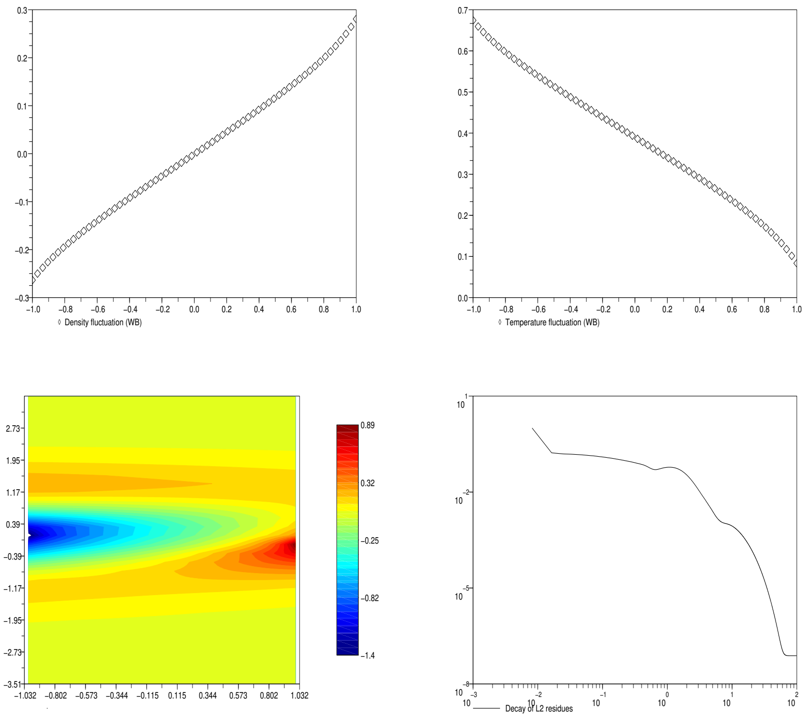

FIGURE 12. Stationary regime at time $t = 100$ for Siewert's test case [60] with $\delta_1 = -\delta_2 = 1$, $\alpha_1 = 0.7$and $\alpha_2 = 0.3$.

macroscopic density (top, left) doesn't show much changes with respect to Fig.10, however the temperature looks much more different (top, right). We stress that our values are completely compatible with the ones found by Siewert (see Table 1 in [60], page 261) using a very different method: in particular, he solves by a least-squares technique the boundary-value problem for the stationary equation (22) with $a = 1$. Finally, we observe that, even on this delicate test-case, our well-balanced Godunov scheme (45)–(46) succeeds in stabilizing onto a physically correct numerical steady-state with monotonically decreasing residues; precisely, the mass and heat flow rates vary between 0 and -3.5×10^{-7}, 0.773610 and 0.773635, respectively. Moreover, the value of the normalized heat flux[7] differs from the one written in [60] (page 262, with $N = 60$ versus $N = 25$ in the present time-marching case) by only 0.17%. The walls have correctly thermalized the gas: such results can be considered satisfying.

5.4. **Sound wave in rarefied gas.** Besides the density and the temperature of the gas which can be computed as indicated in (27), the $(1, 1)$ component of the pressure tensor $p_{1,1}(t, x)$ and the gas pressure $p(t, x)$ can be deduced from Ψ (see *e.g.* [65]),

$$p_{1,1}(t,x) = \frac{1}{\sqrt{\pi}} \int_{\mathbb{R}} \left[(\xi^2 \ 0)^T . \Psi(t,x,\xi) \right] \frac{\exp(-\xi^2)}{\sqrt{\pi}} d\xi,$$

[7]The normalization factor is $\frac{\alpha_1\alpha_2(\delta_1-\delta_2)}{\sqrt{\pi}(\alpha_1+\alpha_2-\alpha_1\alpha_2)}$, see [6].

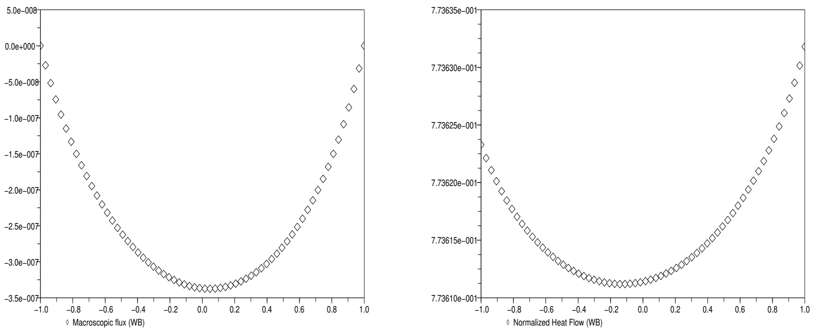

FIGURE 13. Constant quantities: mass flow (left) and heat flow (right).

and respectively,

$$p(t,x) = \frac{1}{3\sqrt{\pi}} \int_{\mathbb{R}} \left[(1+\xi^2 \ 1)^T . \Psi(t,x,\xi) \right] \frac{\exp(-\xi^2)}{\sqrt{\pi}} d\xi.$$

Here, following [65], we have in mind to simulate a transient test-case for which one

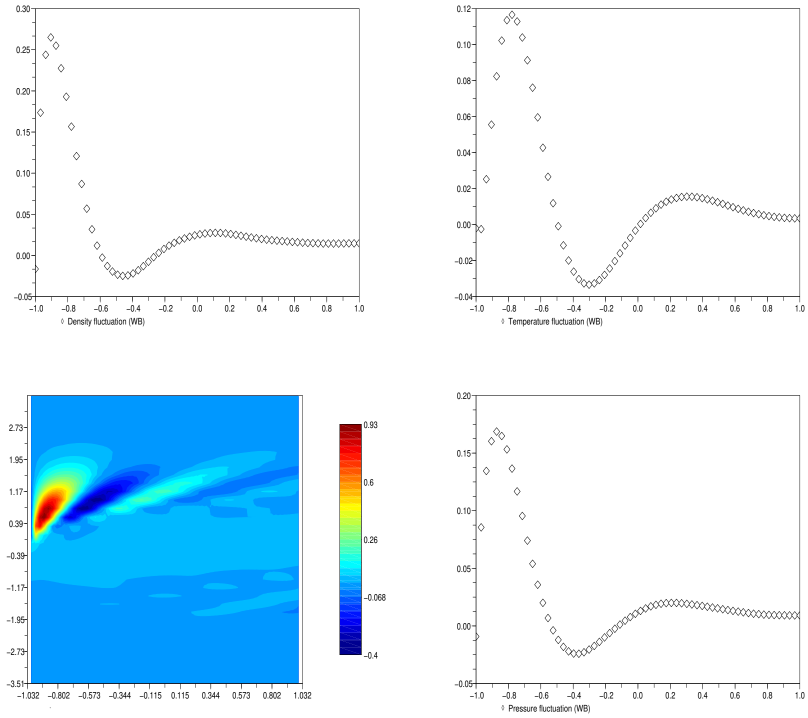

FIGURE 14. Sound wave disturbance with $\alpha = 0.7$ at time $t = 4.35$.

cannot expect a stabilization in large time onto an asymptotic stationary regime with zero macroscopic velocity. Namely, it consists in studying the effects of a sinusoidal vibration of the plate located in $x=-1$ on the gas with the other one in $x=1$ inducing a pure specular reflexion (see Fig.1 in [36]). We decided therefore to set up the well-balanced Godunov scheme (45)–(46), but with the modified matrices adapted to the computation of unsteady regimes which are derived in §A.2 of the Appendix[8]. The inflow boundary condition in $x=-1$ reads for Ψ:

$$\forall t>0, \qquad \Psi(t,-1,|\xi|) = (1-\alpha)\Psi(t,-1,-|\xi|) + \alpha\sqrt{\pi}\sin(3\pi t)\begin{pmatrix} \xi + \frac{\sqrt{\pi}}{2} + \beta \\ 0 \end{pmatrix}.$$

As before, the number β is there to express the fact that the walls located in $x=\pm 1$ are impenetrable to molecules so that no mass flux can exist through each of them. Computing exactly the Gaussian integrals yields the boundary conditions:

$$\begin{aligned}\Psi(t,-1,|\xi|) \quad &= \quad (1-\alpha)\Psi(t,-1,-|\xi|) + \alpha\sqrt{\pi}\sin(3\pi t)\begin{pmatrix} \xi + \frac{\sqrt{\pi}}{2} \\ 0 \end{pmatrix} \\ &\quad + 2\alpha\int_0^\infty \begin{pmatrix} \xi' \\ 0 \end{pmatrix} \Psi(t,-1,-\xi')\exp(-\xi'^2)d\xi'.\end{aligned}$$

Obviously, the specular boundary condition in $x=1$ corresponds to the former one with $\alpha=0$. Numerical results in $t=4.35$ with $\alpha=0.7$ are displayed on Fig. 14: as one can have expected, a pressure rise occurs in the vicinity of the vibrating wall, together with an increase of the density and the temperature. However, these high values get damped quickly with x, the distance measured from the moving wall. No spurious oscillations appear in the approximate numerical values computed by means of our well-balanced Godunov scheme (45)–(46) despite the implementation of a periodic boundary condition.

6. **What happens when the Knudsen number becomes small ?** Up to now, all the considerations have been based onto the linearized problem (6) for which the Knudsen number has been set to unity. However, it is an object of interest to derive numerical schemes able to remain stable and capture the correct fluid behavior as the Knudsen number decreases toward zero (the so–called Euler limit). In this section, we plan to show numerically that this feature is naturally included in our well-balanced strategy; thus we begin by substituting (6) with:

$$\partial_t h + \xi\partial_x h = \frac{1}{\varepsilon}\left(\sum_{i=0}^{4}\int_{\mathbb{R}^3} M(\mathbf{v}')\psi_i(\mathbf{v}')h(t,x,\mathbf{v}')d\mathbf{v}' - h\right). \tag{55}$$

6.1. **A small Knudsen number in the whole domain.** Thanks to our localization process of the source term on a discrete lattice corresponding to cell's interfaces involving the Dirac masses (and the non-conservative products [48]), its action is rendered by means of jump relations across the "zero-waves" which appear in the Riemann solver (see Fig. 3). In order to cope with the correct definition of these zero-waves [1, 32, 33], one has to follow integral curves of the stationary equation for (55), which reads:

$$\varepsilon\partial_x h(x,\mathbf{v}) = \left(\sum_{i=0}^{4}\int_{\mathbb{R}^3} M(\mathbf{v}')\psi_i(\mathbf{v}')h(x,\mathbf{v}')d\mathbf{v}' - h(x,\mathbf{v})\right), \qquad x\in(0,\Delta x). \tag{56}$$

[8]Actually, since the macroscopic flux term is of the order of $0.3 \simeq 10\Delta x$, there is only little difference between these results obtained by means of the modified matrices and the ones one can obtain with the matrices written in §3.3. However, discrepancies may worsen as Δx is decreased.

$N=10$	5.372982
$N=15$	12.20123
$N=25$	155.9844
$N=40$	154.5701

$N=10$	2433.882
$N=15$	809.7012
$N=25$	17667.02
$N=40$	35448.17

Table 2. Condition numbers for the product $\tilde{M}^\varepsilon(M^\varepsilon)^{-1}$ with $\Delta x = 2^{-5}$ (left: $\varepsilon = 0.1$, right: $\varepsilon = 0.01$).

For any value of $\varepsilon > 0$, this equation is solved explicitly by means of the expansion (10) and the elementary solutions (19) and (23). Moreover, we know from §2.4 that such a construction is consistent with the linearized compressible Navier-Stokes equations. Now, in order to handle very easily the values of $\varepsilon \neq 1$, it suffices to observe that the forward-backward problem for (56) is equivalent to the special case $\varepsilon = 1$ considered in this paper, but with $x \in (0, \Delta x/\varepsilon)$. Therefore, the only tiny change to be done inside the well-balanced schemes (38) and (45) is to introduce modified matrices M^ε and $\tilde{M}^\varepsilon$ where all the terms in Δx have to be replaced with $\Delta x/\varepsilon$ in order to compute the interface values (39) and (46). The presence of $\Delta x/\varepsilon$ clearly modifies the condition number of the matrix product $\tilde{M}^\varepsilon\ (M^\varepsilon)^{-1}$ as seen on Table 2. In particular, no restriction appears on Δt despite the stiffness of the collision term. This is reminiscent of the fact that well-balanced schemes are built on NC Riemann solvers for which stiffness cannot create stability issues, as explained in *e.g.* §3.3 of [31]. On Fig.15, we show what happens for the heat transfer test-case with different accommodation coefficients as proposed by Siewert in [60] and already studied in §5.3 (see Fig.12 for comparison with $\varepsilon = 1$). The development of Knudsen's layers is very noticeable when dividing ε by 10. The different values $\alpha_1 \neq \alpha_2$ create an asymmetry in the macroscopic fluxes which effect seems to decrease with ε. When decreasing ε even more, one sees the layers moving closer to the boundaries and hyperbolic waves beginning to emerge inside the computational domain: this is related to the observations in [13, 30] where the "micro-macro" strategy has been used in order to study similar situations. However, from [30], we know that in order to handle very low values of ε, we have to prescribe[9] a time-step $\Delta t \simeq \varepsilon$; we insist on the fact that here, the computational grid and the time-step have been kept **strictly identical** to the ones used in the former cases with $\varepsilon = 1$.

6.2. **A computational domain containing rarefied and fluid areas.** Now we aim at studying what can happen with Siewert's heat transfer test-case when, for instance, the computational domain is split in the following way:

$$\varepsilon = 1 \text{ for } x \in \left(-1, -\frac{1}{3}\right) \cup \left(\frac{1}{3}, 1\right), \qquad \varepsilon = 10^{-2} \text{ for } x \in \left(-\frac{1}{3}, \frac{1}{3}\right). \tag{57}$$

We mainly concentrate on the 2×2 coupled system describing density and temperature fluctuations because similar numerical experiments have been already conducted in [31] on a scalar equation which is very similar to the reduced viscosity equation (14). In particular, it has been observed that, even with a strongly discontinuous opacity coefficient, the well-balanced Godunov scheme was able to numerically stabilize onto a stationary regime with a constant macroscopic flux throughout the whole domain (*c.f.* §3.3). Here, we would like to report on a similar behavior.

[9] At this point, the fact that the well-balanced scheme is completely linear may help for treating it by means of an implicit time-integrator to improve stability.

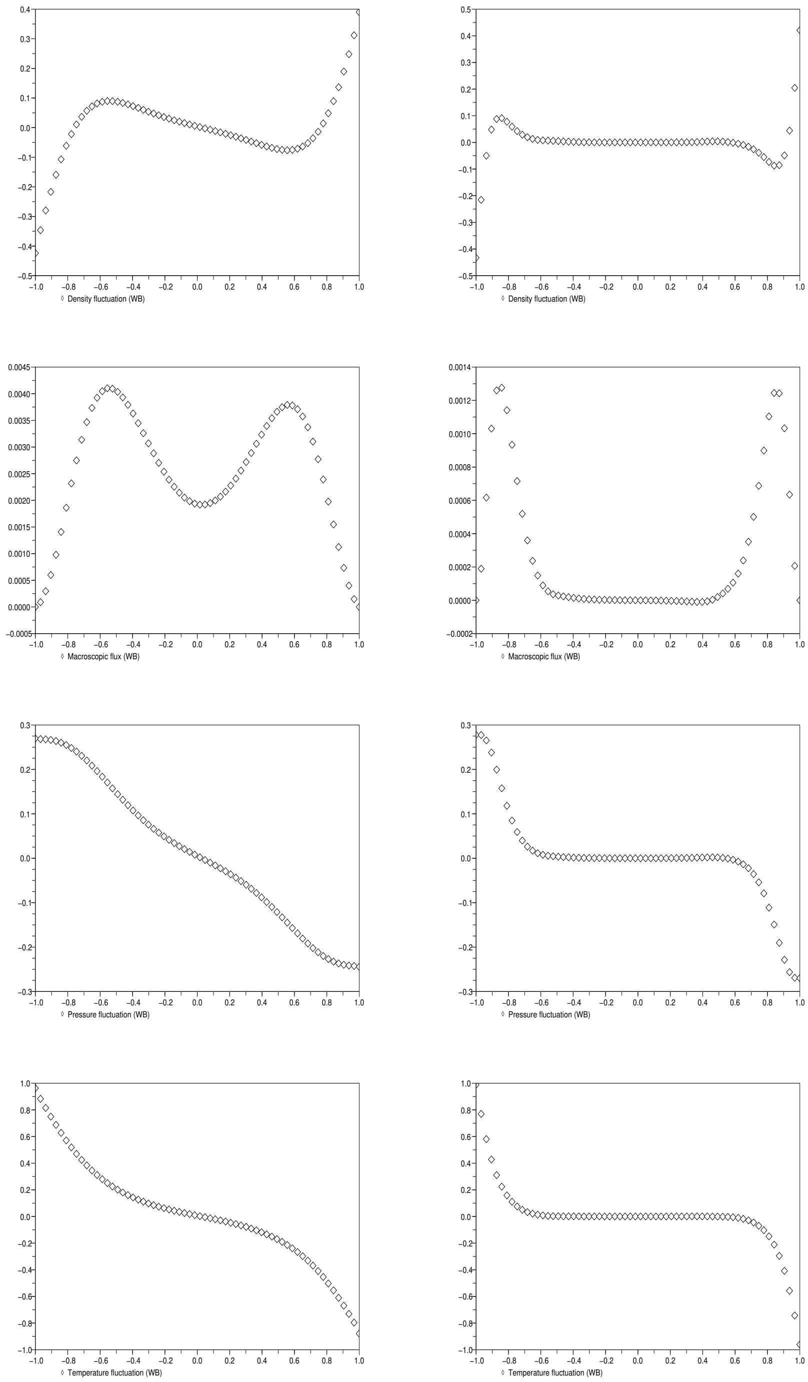

FIGURE 15. Macroscopic quantities $\varrho, \varrho\mathbf{u}_1, p, T$ (top to bottom) for heat transfer at $t = 10$ with $\varepsilon = 10^{-2}$ (left) and $\varepsilon = 10^{-3}$ (right).

Such a test-case aims at displaying that asymptotic-preserving properties hold for

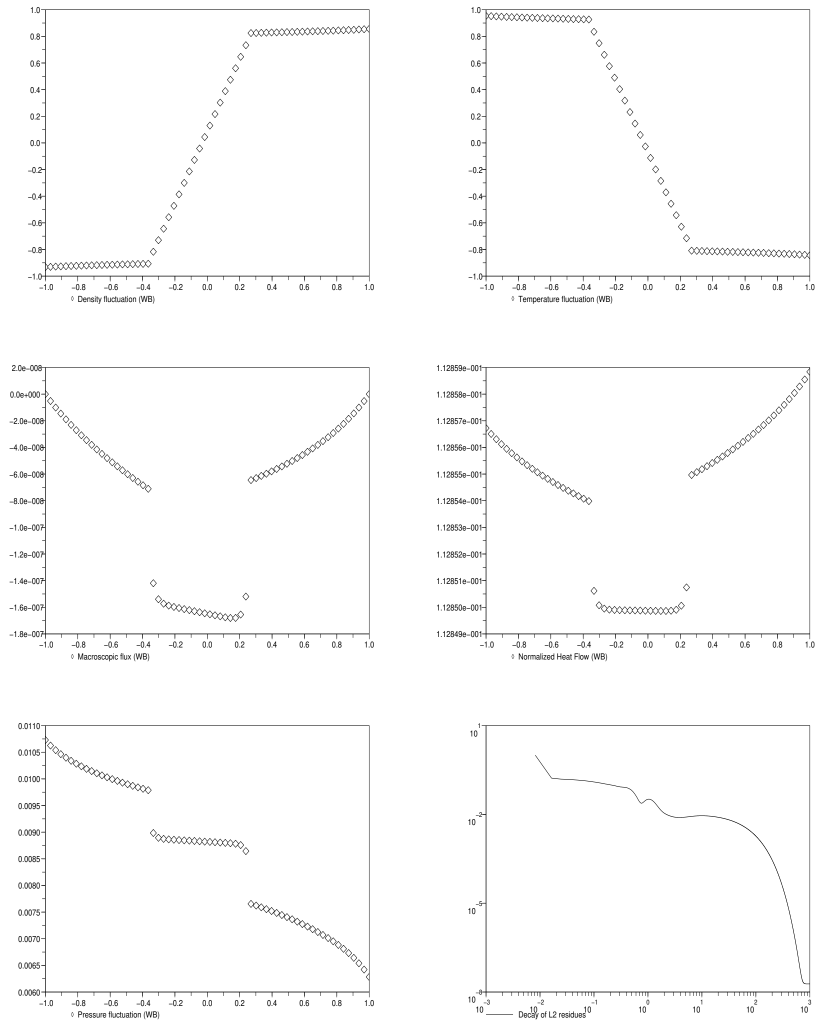

FIGURE 16. Macroscopic quantities ϱ, T (first line), fluxes $\varrho \mathbf{u}_1, q$ (second), pressure p and residues (bottom) for discontinuous ε (57).

the well-balanced Godunov scheme (45)–(46). In particular, no coupling strategy is involved in order to handle the rarefied/fluid areas prescribed by (57). Our strategy is very simple: as in the preceding subsection, we introduce the modified matrices M^ε and $\tilde{M}^\varepsilon$ (where all the terms in Δx have to be replaced with $\Delta x/\varepsilon$) which are used in the "fluid region" located in the middle of the computational domain. In the "rarefied region" (located on both sides close to the walls), we use the usual M, $\tilde{M}$ matrices in order to compute the interface values (46). The outcome of this methodology is shown on Fig.16: the first thing one can notice is the very long time such a mixed problem takes in order to stabilize and reach numerical steady-state. We iterated our scheme up to $t \simeq 1000$ even if $t \simeq 850$ would have probably been sufficient. Even with so many iterations, the residues stall around 10^{-8}, which is acceptable. The remarkable feature is that the numerical mass and heat fluxes (displayed on the middle row of Fig.16) practically stabilized onto a constant value: indeed, they vary between 0 and $-1.7.10^{-7}$, 0.112850 and 0.112859 respectively. This happens despite the strong discontinuity (57) on the Knudsen number ε and the "Lipschitz corners" appearing on the macroscopic density and the temperature (top row of Fig.16). The only quantity which is perhaps not so satisfying is the pressure (bottom line, left) which displays 2 very weak discontinuities at the locations where ε varies: they express the fact that ϱ and T didn't exactly compensate each other in such a way that $p \simeq \varrho T$ would be smooth. However, discontinuities on ϱ and p at the borders between fluid and rarefied regions are initially rather strong thus these 2 remaining jumps appear quite weak in comparison.

7. **Conclusion.** We presented in this paper a global approach to well-balanced schemes for linear models of the Boltzmann equation depending on one space variable only [14]. The general methodology follows the early work by Cercignani on elementary solutions, extending earlier results obtained by Case on neutron transport [15, 16]. We didn't show numerical results on the whole kinetic density $h(t, x, \mathbf{v})$ reconstructed by means of (10) because it is rather straightforward once both Godunov schemes for the reduced viscosity equation (38) and the heat transfer system (45) are implemented. Actually, the critically important point lies in the following fact: the present schemes are **not** of a time-splitting type [52, 53, 54] thus they don't suffer the drawbacks coming inevitably from the dissociation between the dispersive transport step and the collision process which drives the kinetic density function onto a Maxwellian equilibrium distribution.

We stress that the assumption of a solution depending on one space variable only doesn't constitute a severe drawback from the perspective of numerical computations, even in multi-dimension, because the microscopic velocity variable $\mathbf{v}$ is always kept three-dimensional all the way down. Indeed, it is completely possible to set up a finite volumes scheme (for instance on a Cartesian computational grid) and proceed by dimensional (Strang-) splitting. In this context, one faces at each time-step a problem of the same type that has been studied in the present paper for each direction $\mathbf{x}_1$, $\mathbf{x}_2$ and then $\mathbf{x}_3$. Clearly, the kinetic density h would have to be fully reconstructed for each direction in order to be able to update the numerical approximation at the following step. Even in multi-D, finite volume schemes generally involve one-dimensional numerical fluxes, at least at a basic level. In particular, multi-dimensional computations may open the way for attacking the difficult problem of both asymptotic-preserving and well-balanced schemes for the incompressible limit [5, 56] in the same spirit as [31, 32, 33].

Several other kinetic models can be handled by the present framework, at the price of potentially more involved computations. For instance, Barichello, Siewert and collaborators considered 3 different models besides the BGK equation in [57, 58]. Ch. Dalitz derived elementary solutions for certain models of the Boltzmann equation for charged particles in [25, 26]. Fokker-Planck equations are considered in [12] and general parabolic problems in [39].

Acknowledgment: This problem has been suggested by Prof. Giuseppe Toscani in 2003 after the completion of the papers [32, 33].

Appendix A. Balancing steady-states with non-zero macroscopic flux.

A.1. **Details on the stationary equation.** In their papers, Siewert and co-authors study analytically and numerically the stationary equation (22) which is deduced from the original 2×2 heat transfer system by dropping the flux term (21). In this Appendix, we aim at giving some details on this procedure and explain in which circumstances this can be done in a time-dependent well-balanced framework. First, one can easily see (following comments in *e.g.* [59]) that this term has a simple effect on the solution: by using the notation,

$$J := \int_{\mathbb{R}} \xi' \vec{e}_1 . \Psi(x, \xi') \frac{\exp(-|\xi'|^2)}{\sqrt{\pi}} d\xi', \qquad \vec{e}_1 = \begin{pmatrix} 1 \\ 0 \end{pmatrix},$$

and recalling that $\mathbf{P}(-\xi) = \mathbf{P}(\xi)$, one derives the reduced equation (22):

$$\xi \partial_x (\Psi - 2\xi J \vec{e}_1) + (\Psi - 2\xi J \vec{e}_1) = \mathbf{P}(\xi) \int_{\mathbb{R}} \mathbf{P}(\xi')^T (\Psi(x, \xi') - 2\xi' J \vec{e}_1) \frac{\exp(-|\xi'|^2)}{\sqrt{\pi}} d\xi'.$$

Hence the effect of the "flux term" in the complete 2×2 system induces a shifting mechanism of the kinetic density onto the macroscopic flow J. If one assumes that in the geometry of Fig. 2.1, the walls are impenetrable to molecules, then all the realizable equilibrium states of (12) are endowed with a zero macroscopic velocity, meaning that asymptotically, $J = 0$. In the well-balanced terminology for hyperbolic shallow water equations, this is strongly reminiscent of the regime called the "lake at rest steady-state". As long as the initial values aren't too far away, it is fully justified to work with the reduced equation (12) which admits the elementary solutions (23). Later, when setting up the numerical scheme (45), these elementary solutions allow to compute the values at each interface thanks to the matrix $\tilde{M} M^{-1}$ and (46). Roughly speaking, this approach is well-suited for steady-states without macroscopic convection, thus steady-states ruled by diffusion mechanisms.

A.2. **Steady-states with non-zero macroscopic velocity.** However, by relaxing the restriction of "no net flow through the walls", one may retain the possibility of having the well-balanced scheme (45)–(46) to compute kinetic densities whose macroscopic flux doesn't progressively vanish as time increases. Clearly, the elementary solutions (23) become incorrect simply because $(x - \xi)\vec{e}_1$ doesn't satisfy the 2×2 system when the non-zero flux term is included: it has to be substituted with $-\xi \vec{e}_1$. Another change is necessary (as written in [58], formulas (67)):

$$(x - \xi) \begin{pmatrix} \xi^2 - \frac{3}{2} \\ 1 \end{pmatrix} \text{ instead of } (x - \xi) \mathbf{P}(\xi) \vec{e}_1.$$

Concerning the constants of separation ν, they aren't affected by the inclusion of the flux term (21) because we saw that its effect is limited to adding a function linear in ξ. There is no theoretical result of completeness for elementary solutions in this case though. Therefore, in order to set up a well-balanced scheme able to cope with steady-states with non-vanishing macroscopic velocities, it suffices to modify the matrices M and $\tilde{M}$ (as in §3.3) by making the Δx factor disappear (which replaces $\Delta x \pm \boldsymbol{\xi}$ by $\pm \boldsymbol{\xi}$ and also to replace the $(\Delta x \pm \boldsymbol{\xi})(\boldsymbol{\xi}^2 - \frac{1}{2})$ by $(\Delta x \pm \boldsymbol{\xi})(\boldsymbol{\xi}^2 - \frac{3}{2})$ in the column $4N - 1$ only. This procedure can also be extended for variable Knudsen numbers ε as in our previous §6 by substituting Δx by $\Delta x / \varepsilon$. The resulting modified matrices yield a product $\tilde{M}^\varepsilon (M^\varepsilon)^{-1}$ whose condition numbers with respect to N and Δx remains similar to the ones formerly observed: see Table 3.

$N = 10$	1.1715878
$N = 15$	1.2415648
$N = 25$	1.3951388
$N = 40$	1.6624049

$N = 10$	2558.8294
$N = 15$	2438.4454
$N = 25$	8484.6604
$N = 40$	35448.172

TABLE 3. Condition numbers for modified $\tilde{M}^\varepsilon(M^\varepsilon)^{-1}$ with $\Delta x = 2^{-5}$ (left: $\varepsilon = 1$, right: $\varepsilon = 0.01$, compare with Tables 1 and 2).

A.3. **Numerical comparison with time-splitting.** This situation is very similar to what happens in the field of hyperbolic systems of balance laws where the Jacobian of the nonlinear flux function can admit vanishing eigenvalues. In this case, the stationary equations become a differential-algebraic system with singular solutions. The zero eigenvalue of the fluxes interferes with the stationary Dirac mass of the localized source term: this is usually called "nonlinear resonance" [37] and this intricate situation has been systematically excluded in [1]. In the particular case of the Euler equations for a perfect gas, nonlinear resonance can occur at sonic and stagnation points. Here, we observe a similar behavior as the numerical treatment for vanishing macroscopic velocity differs from non-vanishing ones. The critical threshold for switching from one to another may be chosen as $J \simeq \Delta x$, the space-step of the computational grid. Hence we wanted to study the outcomes of both well-balanced strategies on a very simple test-case where boundary conditions lead to a stationary regime with a rather big macroscopic flow:

$$\Psi(x = -1, |\xi|) = \begin{pmatrix} 10 \\ 5 \end{pmatrix}, \qquad \Psi(x = 1, -|\xi|) = \begin{pmatrix} 20 \\ 30 \end{pmatrix}.$$

We compared both results of well-balanced schemes with the ones generated by a standard time-splitting strategy (white squares) at time $t = 24.5$ with $N = 10$ with $\Delta x = 2^{-5}$. They are displayed on Fig.17: in the left column, the well-balanced scheme (45)–(46) and in the right one, a scheme (45) using values from the modified matrices of §A.2 adapted to non-zero macroscopic velocities (dark squares). On the left, one sees an agreement between the two different numerical strategies only for the temperature. The macroscopic density, the mass and heat flows are very different. On the right column, the macroscopic density and the temperature agree; moreover, the mass and heat flow are not only of the same order, but one sees that the time-splitting scheme fails completely at getting them constant. The modified well-balanced approach shows a neat superiority as they appear completely flat.

REFERENCES

[1] D. Amadori, L. Gosse, G. Guerra, *Global BV entropy solutions and uniqueness for hyperbolic systems of balance laws*, Arch. Rational Mech. Anal. **162** (2002) 327–366.

[2] K. Aoki, C. Cercignani, *A technique for time-dependent boundary value problems in the kinetic theory of gases. Part I: Basic analysis*, J. Appl. Math. Phys. (ZAMP) **35** (1984) 127–143.

[3] J. Appell, A.S. Kalitvin, P.P. Zabrejko, *Boundary value problems for integro-differential equations of Barbashin type*, J. Integral Equ. Applic. **6** (1994) 1–30.

[4] A. Arnold, J.A. Carrillo, M.D. Tidriri, *Large-time behavior of discrete equations with non-symmetric interactions*, Math. Mod. Meth. in Appl. Sci. **12** (2002) 1555–1564.

[5] C. Bardos, F. Golse, D. Levermore, *Fluid dynamic limits of kinetic equations. I. Formal derivations*, J. Stat. Phys. **63** (1991) 323–344.

[6] L.B. Barichello, M. Camargo, P. Rodrigues and C.E. Siewert, *Unified Solutions to Classical Flow Problems Based on the BGK Model*, ZAMP **52** (2001) 517-534.

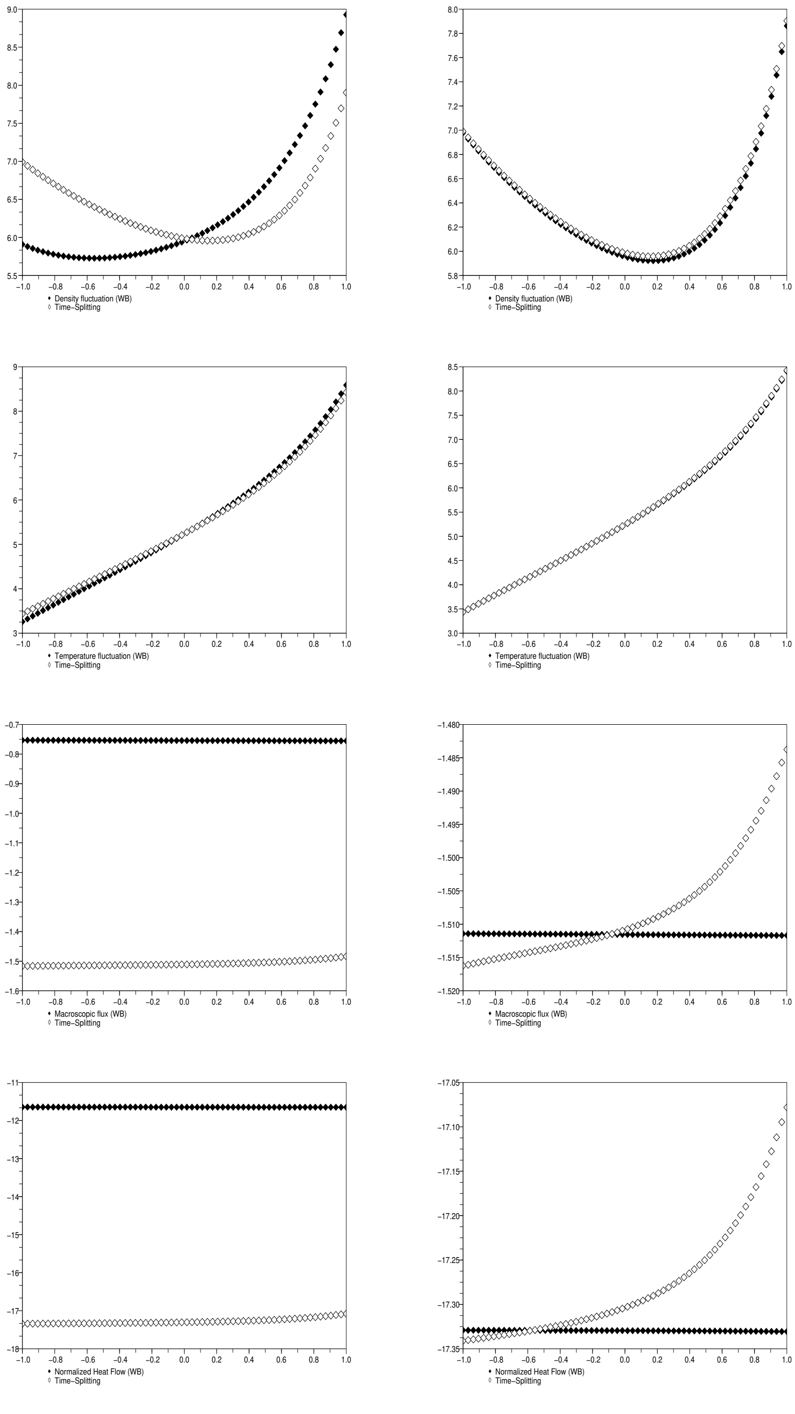

FIGURE 17. Macroscopic density, temperature, mass and heat flow at time $t = 24.5$ (top to bottom) with time-splitting versus (45).

[7] L.B. Barichello C.E. Siewert, *A discrete-ordinates solution for a non-grey model with complete frequency redistribution*, JQSRT **62** (1999) 665–675

[8] G.R. Bart, R.L. Warnock, *Linear integral equations of the third kind*, SIAM J. Math. Anal. **4** 609-622 (1973).

[9] P. Bassanini, C. Cercignani, C.D. Pagani, *Comparison of kinetic theory analyses of linearized heat transfer between parallel plates*, Int. J. Heat Mass Transfer **10** (1967) 447–460.

[10] P. Bassanini, C. Cercignani, C.D. Pagani, *Influence of the accommodation coefficient on the heat transfer in a rarefied gas*, Int. J. Heat Mass Transfer **11** (1968) 1359–1368.

[11] R. Beals, *An abstract treatment of some forward-backward problems of transport and scattering*, J. Funct. Anal. **34** (1979) 1–20.

[12] R. Beals, V. Protopopescu *Half-range completeness for the Fokker-Planck equation*, J. Stat. Phys. **32** (1983) 565–584.

[13] M. Bennoune, M. Lemou, L. Mieussens, *Uniformly stable numerical schemes for the Boltzmann equation preserving the compressible Navier-Stokes asymptotics*, J. Comp. Phys. **227** (2008) 3781–3803.

[14] A. Biryuk, W. Craig, V. Panferov, *Strong solutions of the Boltzmann equation in one spatial dimension*, C.R. Acad. Sci. Paris Ser. I **342** (2006) 843–848.

[15] Kenneth M. Case, *Elementary solutions of the transport equation and their applications*, Ann. Physics **9** (1960) 1–23.

[16] K.M. Case, P.F. Zweifel, **Linear transport theory**, Addison-Wesley series in nuclear engineering (1967).

[17] C. Cercignani, *Elementary solutions of the linearized gas-dynamics Boltzmann equation and their application to the slip-flow problem*, Ann. Physics **20** (1962) 219–233.

[18] C. Cercignani, *Plane Couette flow according to the method of elementary solutions*, J. Math. Anal. Applic. **11** (1965) 93–101.

[19] C. Cercignani, *Methods of solution of the linearized Boltzmann equation for rarefied gas dynamics*, J. Quant. Spectrosc. Radiat. Transfer **11** (1971) 973–985.

[20] C. Cercignani, *Analytic solution of the temperature jump problem for the BGK model*, TTSP **6** (1977) 29.

[21] C. Cercignani, *Solution of a linearized kinetic model for an ultrarelativistic gas*, J. Stat. Phys. **42** (1986) 601–620.

[22] C. Cercignani, **Mathematical methods in kinetic theory**, Plenum, New York (1969).

[23] C. Cercignani, **Slow Rarefied Flows; Theory and Application to Micro-Electro-Mechanical Systems**, Progress in Mathematical Physics, Birkhäuser Verlag (2006).

[24] C. Cercignani and F. Sernagiotto, *The method of elementary solutions for time-dependent problems in linearized kinetic theory*, Ann. Physics **30** (1964) 154–167.

[25] Ch. Dalitz, *Half-space problem of the Boltzmann equation for charged particles*, J. Stat. Phys. **88**. (1997) 129–144.

[26] E. DeGroot, Ch. Dalitz, *Exact solution for a boundary value problem in semiconductor kinetic theory*, J. Math. Phys. **38** (1997) 4629–4643.

[27] L. Desvillettes, *Convergence to equilibrium in large time for Boltzmann and BGK equations*, Arch. Rat. Mech. Anal. **110** (1990) 73–91.

[28] L. Desvillettes, F. Salvarani, *Asymptotic behavior of degenerate linear transport equations*, Bull. Sci. Math. **133** (2009) 848–858.

[29] A. Frangi, A. Frezzotti, S. Lorenzani, *On the application of the BGK kinetic model to the analysis of gas-structure interaction in MEMS*, Computers and Structures **85** (2007) 810–817.

[30] F. Filbet, S. Jin, *A class of asymptotic-preserving schemes for kinetic equations and related problems with stiff sources*, J. Comp. Phys. **229** (2010) 7625-7648

[31] L. Gosse, *Transient radiative transfer in the grey case: well-balanced and asymptotic-preserving schemes built on Case's elementary solutions*, to appear in JQSRT.

[32] L. Gosse, G. Toscani, *An asymptotic-preserving well-balanced scheme for the hyperbolic heat equations*, C.R. Math. Acad. Sci. Paris **334** (2002) 337–342.

[33] L. Gosse, G. Toscani, *Space localization and well-balanced scheme for discrete kinetic models in diffusive regimes*, SIAM J. Numer. Anal. **41** (2003) 641–658.

[34] J. Greenberg, A.Y. LeRoux, *A well balanced scheme for the numerical processing of source terms in hyperbolic equations*, SIAM J. Numer. Anal. **33** (1996) 1 – 16.

[35] W. Greenberg, C.V.M. Van der Mee, P.F. Zweifel, *Generalized kinetic equations*, Integr. Equa. Oper. Theory **7** (1984) 60–95.

[36] N. Hadjiconstantinou, A. Garcia, *Molecular simulations of sound wave propagation in simple gases*, Physics of Fluids **13** (2001) 1040–1046.

[37] E. Isaacson, B. Temple, *Convergence of the 2×2 Godunov method for a general resonant nonlinear balance law*, SIAM J. Appl. Math. **55** (1995) 625-640

[38] Shi Jin, David Levermore, *The discrete-ordinate method in diffusive regimes*, Transp. Theor. Stat. Phys. **20** (1991) 413 - 439.

[39] A Kadir Aziz, D.A. French, S. Jensen, R.B. Kellogg, *Origins, analysis, numerical analysis and numerical approximation of a forward-backward parabolic problem*, MAth. Modell. Numer. Anal. (M2AN) **33** (1999) 895–922.

[40] H. Kaper, *A constructive approach to the solution of a class of boundary value problems of mixed type*, J. Math. Anal. Applic. **63** (1978) 691–718.

[41] H. Kaper, *Boundary value problems of mixed type arising in the kinetic theory of gases*, SIAM J. Math. Anal. **10** (1979) 161–178.

[42] H. Kaper, *Spectral representation of an unbounded linear transformation arising in the kinetic theory of gases*, SIAM J. Math. Anal. **10** (1979) 179–191.

[43] Tomaž Klinc, *On completeness of eigenfunctions of the one-speed transport equation*, Commun. Math. Phys. **41** (1975) 273–279.

[44] G.M. Kremer, **An Introduction to the Boltzmann Equation and Transport Processes in Gases**, Interaction of Mechanics and Mathematics, Springer (2010).

[45] J.T. Kriese, T.S. Chang, C.E. Siewert, *Elementary solutions of coupled model equations in the kinetic theory of gases*, Int. J. Eng. Sci. **12** (1974) 441–470.

[46] A.V. Latyshev, *The use of Case's method to solve the linearized BGK equations for the temperature-jump problem*, Progr. Math. Mech. USSR **54** (1990), 480–484.

[47] A.V. Latyshev, A.A. Yushkanov, *An analytic solution of the problem of the temperature jumps and vapour density over a surface when there is a temperature gradient*, J. Applied Math. Mech. **58** (1994), 259–265.

[48] Ph. LeFloch, A.E. Tzavaras, *Representation of weak limits and definition of nonconservative products*, SIAM J. Math. Anal. **30** (1999), 1309 – 1342.

[49] T.P. Liu, T. Yang, S.H. Yu, *Energy method for Boltzmann equation*, Physica D **188** (2004) 178–192.

[50] T.P. Liu, S.H. Yu, *Boltzmann equation: micro-macro decomposition and positivity of shock profiles*, Comm. Math. Phys. **246** (2004) 133–179.

[51] Taki Ohwada, *Boltzmann schemes for the compressible Navier-Stokes equations*, in **Rarefied gas dynamics: 22nd Internat. Symp.** Edited by T.J. Bartel, M.A. Gallis (2001) 321–328.

[52] L. Pareschi, B. Perthame, *A Fourier spectral method for homogeneous Boltzmann equations*, Transp. Theo. Stat. Phys. **25** (1996) 369–383.

[53] L. Pareschi, G. Russo, *Numerical solution of the Boltzmann equation: I. spectrally accurate approximation of the collision operator*, SIAM J. Numer. Anal. **37** (2000) 1217–1245.

[54] L. Pareschi, G. Russo, *An introduction to the numerical analysis of the Boltzmann equation*, Riv. Mat. Univ. Parma **4** (2005) 145–250.

[55] B. Perthame, *Mathematical tools for kinetic equations*, Bull. Amer. Math. Soc. **41** (2004) 205–244.

[56] L. Saint-Raymond, *From the BGK model to the Navier-Stokes equations*, Ann. Scient. Ec. Norm. Sup. **36** (2003) 271–317.

[57] C.S. Scherer, J.F. Prolo Filho, L.B. Barichello, *An analytical approach to the unified solution of kinetic equations in rarefied gas dynamics. I Flow problems*, ZAMP **60** (2009) 70–115.

[58] C.S. Scherer, J.F. Prolo Filho, L.B. Barichello, *An analytical approach to the unified solution of kinetic equations in rarefied gas dynamics. II Heat transfer problems*, ZAMP **60** (2009) 651–687.

[59] C.E. Siewert, *Half-space analysis basic to the linearized Boltzmann equation*, ZAMP **28** (1977) 531–535 (Brief reports).

[60] C.E. Siewert, *A discrete-ordinates solution for heat transfer in a plane channel*, J. Comp. Phys. **152** (1999) 251–263.

[61] C.E. Siewert, E.E. Burniston, *Half-space analysis basic to the time-dependent BGK model in the kinetic theory of gases*, J. Math. Phys. **18** (1977) 376–380.

[62] C.E. Siewert, E.E. Burniston, J.R. Thomas, Jr. *Discrete spectrum basic to kinetic theory*, Phys. Fluids **16** (1971) 1532–1533.

[63] C.E. Siewert, J. T. Kriese, *Half-space orthogonality relations basic to the solution of time-dependent boundary value problems in the kinetic theory of gases*, ZAMP **29** (1978) 199–205.

[64] C.E. Siewert, S.J. Wright *Efficient eigenvalue calculations in radiative transfer*, J. Quant. Spectro. Radiat. Transf. (1999) 685–688.

[65] J.R. Thomas, C.E. Siewert, *Sound wave propagation in a rarefied gas*, Transp. Theory Stat. Phys. **8** (1979) 219–240.

[66] A.E. Tzavaras, *On the mathematical theory of fluid dynamic limits to conservation laws* In: **Advances in Mathematical Fluid Mechanics**, J. Malek, J. Nečas and M. Rokyta, eds.; Springer, New York, (2000) 192–222

[67] C. Van der Mee, **Exponentially dichotomous operators and applications** Birkhäuser (2008) (ISBN 203764387319).

[68] C. Van der Mee, C.E. Siewert *On unbounded eigenvalues in transport theory*, ZAMP **34** (1983) 556–561.

[69] C. Villani *A review of mathematical topics in collisional kinetic theory*, Handbook of Mathematical Fluid Dynamics **1**, North Holland, (2002) 71–305

[70] M.M.R. Williams, *A review of the rarefied gas dynamics theory associated with some classical problems in flow and heat Transfer*, Z. Angew. Math. Phys. **52** (2001) 500-516.

E-mail address: `l.gosse@ba.iac.cnr.it`